

# Maximally Symmetric Two Higgs Doublet Model with Natural Standard Model Alignment

---

P. S. Bhupal Dev<sup>a</sup> and Apostolos Pilaftsis<sup>a,b</sup>

<sup>a</sup> *Consortium for Fundamental Physics, School of Physics and Astronomy,  
University of Manchester, Manchester, M13 9PL, United Kingdom*

<sup>b</sup> *CERN, Department of Physics, Theory Division, CH-1211 Geneva 23, Switzerland*

**ABSTRACT:** We study the Higgs mass spectrum as predicted by a Maximally Symmetric Two Higgs Doublet Model (MS-2HDM) potential based on the  $SO(5)$  group, softly broken by bilinear Higgs mass terms. We show that the lightest Higgs sector resulting from this MS-2HDM becomes naturally aligned with that of the Standard Model (SM), independently of the charged Higgs boson mass and  $\tan\beta$ . In the context of Type-II 2HDM,  $SO(5)$  is the simplest of the *three* possible symmetry realizations of the scalar potential that can naturally lead to the SM alignment. Nevertheless, renormalization group effects due to the hypercharge gauge coupling  $g'$  and third-generation Yukawa couplings may break sizeably this alignment in the MS-2HDM, along with the custodial symmetry inherited by the  $SO(5)$  group. Using the current Higgs signal strength data from the LHC, which disfavour large deviations from the SM alignment limit, we derive lower mass bounds on the heavy Higgs sector as a function of  $\tan\beta$ , which can be stronger than the existing limits for a wide range of parameters. In particular, we propose a new collider signal based on the observation of four top quarks to directly probe the heavy Higgs sector of the MS-2HDM during the run-II phase of the LHC.

**KEYWORDS:** Higgs Physics, Beyond Standard Model

---

## Contents

<b>1</b>	<b>Introduction</b>	<b>1</b>
<b>2</b>	<b>Maximally Symmetric Two Higgs Doublet Model Potential</b>	<b>3</b>
2.1	Custodial Symmetries in the MS-2HDM	5
2.2	Scalar Spectrum in the MS-2HDM	6
<b>3</b>	<b>RG and Soft Breaking Effects</b>	<b>7</b>
<b>4</b>	<b>Misalignment Predictions</b>	<b>11</b>
<b>5</b>	<b>Collider Signals</b>	<b>14</b>
5.1	Branching Fractions	14
5.2	Charged Higgs Signal	14
5.3	Heavy Neutral Higgs Signal	18
<b>6</b>	<b>Conclusions</b>	<b>22</b>
<b>A</b>	<b>Higgs Spectrum and Couplings in a General 2HDM</b>	<b>23</b>
<b>B</b>	<b>Two-loop RGEs in a General 2HDM</b>	<b>25</b>

---

## 1 Introduction

The discovery of a Higgs resonance with mass around 125 GeV at the LHC [1, 2] offers an unprecedented opportunity for probing extended Higgs scenarios beyond the Standard Model (SM). Although the measured properties of the discovered Higgs boson show remarkable consistency with those predicted by the SM [3, 4], the current experimental data still leave open the possibility of new physics that results from an extended Higgs sector. In fact, several well-motivated new-physics scenarios require an enlarged Higgs sector, such as supersymmetry [5], in order to address a number of theoretical and cosmological issues, including the gauge hierarchy problem, the origin of the Dark Matter and the baryon asymmetry in our Universe. Here we follow a modest bottom-up approach and consider one of the simplest Higgs-sector extensions of the SM, namely the Two Higgs Doublet Model (2HDM) [6].

The 2HDM contains two complex scalar fields transforming as iso-doublets  $(\mathbf{2}, 1)$  under the SM electroweak gauge group  $SU(2)_L \otimes U(1)_Y$ :

$$\Phi_i = \begin{pmatrix} \phi_i^+ \\ \phi_i^0 \end{pmatrix}, \quad (1.1)$$

with  $i = 1, 2$ . In this doublet field space  $\Phi_{1,2}$ , the general 2HDM potential reads

$$\begin{aligned}
V = & -\mu_1^2(\Phi_1^\dagger\Phi_1) - \mu_2^2(\Phi_2^\dagger\Phi_2) - \left[ m_{12}^2(\Phi_1^\dagger\Phi_2) + \text{H.c.} \right] \\
& + \lambda_1(\Phi_1^\dagger\Phi_1)^2 + \lambda_2(\Phi_2^\dagger\Phi_2)^2 + \lambda_3(\Phi_1^\dagger\Phi_1)(\Phi_2^\dagger\Phi_2) + \lambda_4(\Phi_1^\dagger\Phi_2)(\Phi_2^\dagger\Phi_1) \\
& + \left[ \frac{1}{2}\lambda_5(\Phi_1^\dagger\Phi_2)^2 + \lambda_6(\Phi_1^\dagger\Phi_1)(\Phi_1^\dagger\Phi_2) + \lambda_7(\Phi_1^\dagger\Phi_2)(\Phi_2^\dagger\Phi_2) + \text{H.c.} \right], \quad (1.2)
\end{aligned}$$

which contains four real mass parameters  $\mu_{1,2}^2$ ,  $\text{Re}(m_{12}^2)$ ,  $\text{Im}(m_{12}^2)$ , and ten real quartic couplings  $\lambda_{1,2,3,4}$ ,  $\text{Re}(\lambda_{5,6,7})$ , and  $\text{Im}(\lambda_{5,6,7})$ . As a consequence, the vacuum structure of the general 2HDM can be quite rich [7], and in principle, can allow for a wide range of parameter space still compatible with the existing LHC constraints. However, additional requirements, such as the Glashow–Weinberg condition [8, 9], must be imposed, so as to avoid Higgs interactions with unacceptably large flavour changing neutral currents (FCNC) at the tree level. The Glashow–Weinberg condition is satisfied by four discrete choices of tree-level Yukawa couplings between the Higgs doublets and SM fermions.<sup>1</sup> By performing global fits to the current Higgs signals at the LHC and Tevatron in terms of the 2HDM parameter space, it has been shown [11–18] that all four discrete 2HDM types are constrained to lie close to the so-called SM *alignment limit*, in which the mass eigenbasis of the CP-even scalar sector aligns with the SM gauge eigenbasis. Specifically, in the Type-II (MSSM-type) 2HDM, the coupling of the SM-like Higgs to vector bosons is constrained to lie within 10% of the SM value at 95% CL [14, 19–22].

In light of the present and upcoming LHC data, possible mechanisms that lead to the SM alignment limit within the 2HDM require further investigation and scrutiny. Naively, the SM alignment limit is often associated with the decoupling limit, in which all the non-standard Higgs bosons are assumed to be much heavier than the electroweak scale so that the lightest CP-even scalar behaves like the SM Higgs boson. This SM alignment limit can also be achieved, without decoupling [23–26].<sup>2</sup> However, for small  $\tan\beta$  values, this is usually attributed to accidental cancellations in the 2HDM potential [26].

In this paper, we seek a symmetry of the 2HDM potential to naturally justify the alignment limit, without decoupling, independently of the kinematic parameters of the theory, such as the charged Higgs mass and  $\tan\beta$ . We show that a Maximally Symmetric 2HDM (MS-2HDM) potential based on the SO(5) group can *naturally* realize the alignment limit, where SO(5) acts on a bilinear field space to be discussed in Section 2. In Section 3, we show that, in the context of Type-II 2HDM, the maximal symmetry group SO(5) is the simplest of the *three* possible symmetry realizations of the scalar potential having natural alignment. Nevertheless, as we analyze in Section 3, renormalization group (RG) effects due to the hypercharge gauge coupling  $g'$  and third-generation Yukawa couplings, as well as soft-breaking mass parameters, violate explicitly the SO(5) symmetry, thereby inducing relevant deviations from the alignment limit. As we discuss in Section 4, such deviations

<sup>1</sup>In general, the absence of tree-level flavour-changing couplings of the neutral scalar fields can be guaranteed by requiring the Yukawa coupling matrices to be aligned in flavour space [10].

<sup>2</sup>A similar situation was also discussed in an extension of the MSSM with a triplet scalar field [27], where alignment without decoupling could be achieved in a parameter region at small  $\tan\beta \lesssim 10$ .

lead to distinct predictions for the Higgs spectrum of the MS-2HDM. In Section 5, we present a novel collider signature of the MS-2HDM with four top quarks as final states. In Section 6 we present our conclusions. Finally, several technical details related to our study have been relegated to Appendices A and B.

## 2 Maximally Symmetric Two Higgs Doublet Model Potential

In order to identify all accidental symmetries of the 2HDM potential, it is convenient to introduce the 8-dimensional complex multiplet [7, 28, 29]:

$$\mathbf{\Phi} \equiv \begin{pmatrix} \Phi_1 \\ \Phi_2 \\ \tilde{\Phi}_1 \\ \tilde{\Phi}_2 \end{pmatrix}, \quad (2.1)$$

where  $\tilde{\Phi}_i = i\sigma^2\Phi_i^*$  (with  $i = 1, 2$ ) and  $\sigma^2$  is the second Pauli matrix. We should remark that the complex multiplet  $\mathbf{\Phi}$  satisfies the Majorana property [7]:  $\mathbf{\Phi} = C\mathbf{\Phi}^*$ , where  $C = \sigma^2 \otimes \sigma^0 \otimes \sigma^2$  is the charge-conjugation matrix, with  $\sigma^0 = \mathbf{1}_{2 \times 2}$  being the identity matrix. In terms of the  $\mathbf{\Phi}$ -multiplet, the following *null* 6-dimensional Lorentz vector can be defined [7, 29]:

$$R^A \equiv \mathbf{\Phi}^\dagger \Sigma^A \mathbf{\Phi}, \quad (2.2)$$

where  $A = 0, 1, \dots, 5$  and the six  $8 \times 8$ -dimensional matrices  $\Sigma^A$  may be expressed in terms of the three Pauli matrices  $\sigma^{1,2,3}$ , as follows:

$$\begin{aligned} \Sigma^{0,1,3} &= \frac{1}{2}\sigma^0 \otimes \sigma^{0,1,3} \otimes \sigma^0, & \Sigma^2 &= \frac{1}{2}\sigma^3 \otimes \sigma^2 \otimes \sigma^0, \\ \Sigma^4 &= -\frac{1}{2}\sigma^2 \otimes \sigma^2 \otimes \sigma^0, & \Sigma^5 &= -\frac{1}{2}\sigma^1 \otimes \sigma^2 \otimes \sigma^0. \end{aligned} \quad (2.3)$$

We must emphasize here that the bilinear field space spanned by the 6-vector  $R^A$  realizes an *orthochronous*  $\text{SO}(1,5)$  symmetry group.

In terms of the 6-vector  $R^A$  defined in (2.2), the 2HDM potential  $V$  given in (1.2) takes on a simple quadratic form:

$$V = -\frac{1}{2}M_A R^A + \frac{1}{4}L_{AB} R^A R^B, \quad (2.4)$$

where  $M_A$  and  $L_{AB}$  are  $\text{SO}(1,5)$  constant ‘tensors’ that depend on the mass parameters and quartic couplings of the scalar potential  $V$  and their explicit forms may be found in [29–32]. Requiring that the  $\text{SU}(2)_L$  gauge-kinetic term of the multiplet  $\mathbf{\Phi}$  remains canonical restricts the allowed set of rotations from  $\text{SO}(1,5)$  to  $\text{SO}(5)$ ,<sup>3</sup> where only the spatial components  $R^I$  (with  $I = 1, \dots, 5$ ) transform, whereas the zeroth component  $R^0$  remains invariant. Consequently, in the absence of the hypercharge gauge coupling  $g'$  and

<sup>3</sup>We note in passing that if the restriction of  $\text{SU}(2)_L$  gauge invariance is lifted, the 2HDM is then equivalent to an *ungauged* theory with 8 real scalars and so the maximal symmetry group becomes the larger group  $\text{O}(8)$  [33].

fermion Yukawa couplings, the maximal symmetry group of the 2HDM is  $G_{2\text{HDM}}^R = \text{SO}(5)$ . Given the group isomorphism  $\text{SO}(5) \sim \text{Sp}(4)/\mathbb{Z}_2$ , the maximal symmetry group of the 2HDM in the original  $\Phi$ -field space is [29]<sup>4</sup>

$$G_{2\text{HDM}}^\Phi = (\text{Sp}(4)/\mathbb{Z}_2) \otimes \text{SU}(2)_L, \quad (2.5)$$

in the custodial symmetry limit of vanishing  $g'$  and fermion Yukawa couplings. The quotient factor  $\mathbb{Z}_2$  in (2.5) is needed to avoid double covering the group  $G_{2\text{HDM}}^\Phi$  in the  $\Phi$ -space. One may note here that the 10 Lie generators of  $\text{Sp}(4)$  may be represented in the  $\Phi$ -space as  $K^a = \kappa^a \otimes \sigma^0$  (with  $a = 0, 1, 2, \dots, 9$ ), where

$$\begin{aligned} \kappa^0 &= \frac{1}{2} \sigma^3 \otimes \sigma^0, & \kappa^1 &= \frac{1}{2} \sigma^3 \otimes \sigma^1, \\ \kappa^2 &= \frac{1}{2} \sigma^0 \otimes \sigma^2, & \kappa^3 &= \frac{1}{2} \sigma^3 \otimes \sigma^3, \\ \kappa^4 &= \frac{1}{2} \sigma^1 \otimes \sigma^0, & \kappa^5 &= \frac{1}{2} \sigma^1 \otimes \sigma^3, \\ \kappa^6 &= \frac{1}{2} \sigma^2 \otimes \sigma^0, & \kappa^7 &= \frac{1}{2} \sigma^2 \otimes \sigma^3, \\ \kappa^8 &= \frac{1}{2} \sigma^1 \otimes \sigma^1, & \kappa^9 &= \frac{1}{2} \sigma^2 \otimes \sigma^1, \end{aligned} \quad (2.6)$$

with the normalization:  $\text{Tr}(\kappa^a \kappa^b) = \delta^{ab}$ . Thus, the group  $G_{2\text{HDM}}^\Phi$  includes the  $\text{U}(1)_Y$  hypercharge group through the  $\text{Sp}(4)$  generator  $K^0$ , whereas the 9 other  $\text{Sp}(4)$  generators listed in (2.6) are related to various Higgs Family and CP transformations [29]. On the other hand, the  $\text{SU}(2)_L$  generators in the  $\Phi$ -space may be written as  $\sigma^0 \otimes \sigma^0 \otimes (\sigma^b/2)$  (with  $b = 1, 2, 3$ ), which manifestly commute with all  $\text{Sp}(4)$  generators  $K^a$ .

As we will see below by an explicit construction [cf. (2.9) and Section 2.1], it is not difficult to deduce that, in the custodial symmetry limit, the maximal symmetry group for an  $n$  Higgs Doublet Model ( $n\text{HDM}$ ) will be

$$G_{n\text{HDM}}^\Phi = (\text{Sp}(2n)/\mathbb{Z}_2) \otimes \text{SU}(2)_L, \quad (2.7)$$

in which case the multiplet  $\Phi$  becomes a Majorana  $4n$ -dimensional complex vector.<sup>5</sup> It is interesting to note that for the SM with  $n = 1$  Higgs doublet, (2.7) yields the well-known result:  $G_{\text{SM}}^\Phi = (\text{SU}(2)_C/\mathbb{Z}_2) \otimes \text{SU}(2)_L$ , by virtue of the group isomorphism:  $\text{Sp}(2) \sim \text{SU}(2)_C$ , where  $\text{SU}(2)_C$  is the custodial symmetry group originally introduced in [36]. Hence, it is important to stress that (2.7) represents a general result that holds for any  $n\text{HDM}$ .

We may now identify all maximal symmetries of the 2HDM potential by classifying all proper, improper and semi-simple subgroups of  $\text{SO}(5)$  in the bilinear  $R^I$  space. In this way, it was found [7, 29] that a 2HDM potential invariant under  $\text{SU}(2)_L \otimes \text{U}(1)_Y$  can

<sup>4</sup>In [29], the symplectic group  $\text{Sp}(4)$  is denoted as  $\text{SU}_M(4)$ , where the 10 generators of the restricted  $\text{U}(4)$  group satisfying a Majorana (symplectic) condition were presented.

<sup>5</sup>Given an apparently deep connection between  $\text{SO}(2n+1)$  and  $\text{Sp}(2n)$  groups [34, 35], both of which have  $n(2n+1)$  generators, one might be able to identify the necessary bilinears in the  $R$ -space for any  $n\text{HDM}$ . However, this is somewhat non-trivial for  $n \geq 3$ , and therefore, we postpone this discussion to a future dedicated study.

possess a maximum of 13 accidental symmetries. This symmetry classification extends the previous list of six symmetries reported in [31], where possible custodial symmetries of the theory were not included. Each of the 13 classified symmetries puts some restrictions on the kinematic parameters appearing in the 2HDM potential (1.2). In a specific diagonally reduced bilinear basis [37, 38], one has the general restrictions  $\text{Im}(\lambda_5) = 0$  and  $\lambda_6 = \lambda_7$ , thus reducing the number of independent quartic couplings to seven. In the maximally symmetric  $\text{SO}(5)$  ( $\sim \text{Sp}(4)/\mathbb{Z}_2$ ) limit, we have the following relations between the scalar potential parameters [7, 29]:

$$\begin{aligned} \mu_1^2 &= \mu_2^2, & m_{12}^2 &= 0, \\ \lambda_2 &= \lambda_1, & \lambda_3 &= 2\lambda_1, & \lambda_4 &= \text{Re}(\lambda_5) = \lambda_6 = \lambda_7 = 0. \end{aligned} \quad (2.8)$$

Thus, in the  $\text{SO}(5)$  limit, the 2HDM potential (1.2) is parametrized by a *single* mass parameter  $\mu^2$  and a *single* quartic coupling  $\lambda$ :

$$\begin{aligned} V &= -\mu^2 \left( |\Phi_1|^2 + |\Phi_2|^2 \right) + \lambda \left( |\Phi_1|^2 + |\Phi_2|^2 \right)^2 \\ &= -\frac{\mu^2}{2} \Phi^\dagger \Phi + \frac{\lambda}{4} (\Phi^\dagger \Phi)^2. \end{aligned} \quad (2.9)$$

It is worth stressing that the MS-2HDM scalar potential in (2.9) is more minimal than the respective potential of the MSSM at the tree level. Even in the custodial symmetric limit  $g' \rightarrow 0$ , the latter only possesses a smaller symmetry:  $\text{O}(2) \otimes \text{O}(3) \subset \text{SO}(5)$ , in the 5-dimensional bilinear  $R^I$  space.

## 2.1 Custodial Symmetries in the MS-2HDM

It is now interesting to discuss the implications of custodial symmetries for the Yukawa sector of the 2HDM. To this end, let us only consider the quark Yukawa sector of the theory, even though it is straightforward to extend our results to the lepton sector as well. The relevant part of the quark-Yukawa Lagrangian in the 2HDM can generally be written down as follows:

$$\begin{aligned} -\mathcal{L}_Y^q &= \bar{Q}_L (h_1^u \tilde{\Phi}_1 + h_2^u \tilde{\Phi}_2) u_R + \bar{Q}_L (h_1^d \Phi_1 + h_2^d \Phi_2) d_R \\ &= (\bar{u}_L, \bar{d}_L) \left( \tilde{\Phi}_1, \tilde{\Phi}_2, \Phi_1, \Phi_2 \right) \mathcal{H} \begin{pmatrix} u_R \\ d_R \end{pmatrix}, \end{aligned}$$

where  $Q_L \equiv (u_L, d_L)^\top$  is the SM quark iso-doublet and we have introduced a  $12 \times 6$ -dimensional *non-square* Yukawa coupling matrix

$$\mathcal{H} \equiv \begin{pmatrix} h_1^u & \mathbf{0}_{3 \times 3} \\ h_2^u & \mathbf{0}_{3 \times 3} \\ \mathbf{0}_{3 \times 3} & h_1^d \\ \mathbf{0}_{3 \times 3} & h_2^d \end{pmatrix}. \quad (2.10)$$

All the custodial symmetries of the 2HDM potential can be deduced by examining the  $\text{Sp}(4)$  generators  $K^a = \kappa^a \otimes \sigma^0$  in the  $\Phi$ -space, where  $\kappa^a$  are explicitly given in (2.6).

Candidate  $\text{Sp}(4)$  generators of the custodial symmetry are those generators that do *not* commute with the hypercharge generator  $K^0$ , i.e.  $K^a$  with  $a = 4, 5, 6, 7, 8, 9$ . It is not difficult to see that these six generators, together with  $K^0$ , form *three* inequivalent realizations of the  $\text{SU}(2)_C$  custodial symmetry [29]: (i)  $K^{0,4,6}$ , (ii)  $K^{0,5,7}$  and (iii)  $K^{0,8,9}$ .

In order to see the implications of the three custodial symmetries (i), (ii) and (iii) for the quark Yukawa sector, we impose a symmetry commutation relation on  $\mathcal{H}$  after generalizing it for *non*-square matrices:

$$\kappa^a \mathcal{H} - \mathcal{H} t^b = \mathbf{0}_{4 \times 2}, \quad (2.11)$$

where  $\mathcal{H}$  is expressed in the reduced  $4 \times 2$ -dimensional space, in which the  $3 \times 3$  flavour space has been suppressed. In addition, we denote with  $t^b = \sigma^b/2$  (with  $b = 1, 2, 3$ ) the three  $2 \times 2$  generators of the custodial  $\text{SU}(2)_C$  group. One can immediately check that it holds  $\kappa^0 \mathcal{H} - \mathcal{H} t^3 = \mathbf{0}_{4 \times 2}$ , which implies that the specific block structure of  $\mathcal{H}$  in (2.10) respects  $\text{U}(1)_Y$  by construction, given the correspondence:  $\kappa^0 \leftrightarrow t^3$ . In detail, imposing (2.11) for the three  $\text{SU}(2)_C$  symmetries, we obtain the following relations among the  $3 \times 3$  up- and down-type quark Yukawa coupling matrices:

$$\begin{aligned} \text{(i)} \quad & h_1^u = e^{i\theta} h_1^d \quad \text{and} \quad h_2^u = e^{i\theta} h_2^d, \\ \text{(ii)} \quad & h_1^u = e^{i\theta} h_1^d \quad \text{and} \quad h_2^u = -e^{i\theta} h_2^d, \\ \text{(iii)} \quad & h_1^u = e^{i\theta} h_2^d \quad \text{and} \quad h_2^u = e^{-i\theta} h_1^d, \end{aligned} \quad (2.12)$$

where  $\theta$  is an arbitrary angle unspecified by the symmetry constraint (2.11). We should stress again that only for a fully  $\text{SO}(5)$ -symmetric 2HDM, the three sets of solutions in (2.12) are equivalent. However, this is not in general true for scenarios that happen to realize only subgroups of  $\text{SO}(5)$ , according to the symmetry classification given in [7, 29].

## 2.2 Scalar Spectrum in the MS-2HDM

The masses and mixing in the Higgs sector of a general 2HDM are given in Appendix A. After electroweak symmetry breaking in the MS-2HDM, we have the breaking pattern

$$\text{SO}(5) \xrightarrow{\langle \Phi_{1,2} \rangle \neq 0} \text{SO}(4), \quad (2.13)$$

which gives rise to a Higgs boson  $H$  with mass  $M_H^2 = 2\lambda_2 v^2$ , whilst the remaining four scalar fields, denoted hereafter as  $h$ ,  $a$  and  $h^\pm$ , are massless (pseudo)-Goldstone bosons. The latter is a consequence of the Goldstone theorem [39] and can be readily verified by means of (2.8) in (A.5). Thus, we identify  $H$  as the SM-like Higgs boson with the mixing angle  $\alpha = \beta$  [cf. (A.7)]. We call this the SM *alignment limit*, which can be naturally attributed to the  $\text{SO}(5)$  symmetry of the theory.

In the exact  $\text{SO}(5)$ -symmetric limit, the scalar spectrum of the MS-2HDM is experimentally unacceptable, as the four massless pseudo-Goldstone particles, viz.  $h$ ,  $a$  and  $h^\pm$ , have sizeable couplings to the SM  $Z$  and  $W^\pm$  bosons [cf. (A.9)]. These couplings induce additional decay channels, such as  $Z \rightarrow ha$  and  $W^\pm \rightarrow h^\pm h$ , which are experimentally excluded [40]. Nevertheless, as we will see in the next section, the  $\text{SO}(5)$  symmetry of the

original theory may be violated predominantly by RG effects due to  $g'$  and third-generation Yukawa couplings, as well as by soft SO(5)-breaking mass parameters, thereby lifting the masses of these pseudo-Goldstone particles.

### 3 RG and Soft Breaking Effects

As discussed in the previous section, the SO(5) symmetry that governs the MS-2HDM will be broken due to  $g'$  and Yukawa coupling effects, similar to the breaking of custodial symmetry in the SM. Therefore, an interesting question will be to explore whether these effects are sufficient to yield a viable Higgs spectrum at the weak scale. To address this question in a technically natural manner, we assume that the SO(5) symmetry is realized at some high scale  $\mu_X$ . The physical mass spectrum at the electroweak scale is then obtained by the RG evolution of the 2HDM parameters given by (1.2). Using state-of-the-art two-loop RG equations given in Appendix B, we examine the deviation of the Higgs spectrum from the SO(5)-symmetric limit due to  $g'$  and Yukawa coupling effects. This is illustrated in Figure 1 for a typical choice of parameters in a Type-II realization of the 2HDM, even though the conclusions drawn from this figure have more general applicability. In particular, we obtain the following breaking pattern starting from a  $SU(2)_L$ -gauged theory:

$$\begin{aligned}
SO(5) \otimes SU(2)_L &\xrightarrow{g' \neq 0} O(3) \otimes O(2) \otimes SU(2)_L \sim O(3) \otimes U(1)_Y \otimes SU(2)_L \\
&\xrightarrow{\text{Yukawa}} O(2) \otimes U(1)_Y \otimes SU(2)_L \sim U(1)_{\text{PQ}} \otimes U(1)_Y \otimes SU(2)_L \\
&\xrightarrow{\langle \Phi_{1,2} \rangle \neq 0} U(1)_{\text{em}} , \tag{3.1}
\end{aligned}$$

where  $U(1)_{\text{em}}$  is the electromagnetic group. In other words, RG-induced  $g'$  effects only lift the charged Higgs-boson mass  $M_{h^\pm}$ , while the corresponding Yukawa coupling effects also lift slightly the mass of the non-SM CP-even pseudo-Goldstone boson  $h$ . However, they still leave the CP-odd scalar  $a$  massless (see left panel of Figure 1 for  $m_{12}^2 = 0$ ), which can be identified as a  $U(1)_{\text{PQ}}$  axion [41]. The deviation of the scalar quartic couplings from the SO(5)-symmetric limit given in (2.8), thanks to  $g'$  and Yukawa coupling effects, is illustrated in Figure 1 (right panel) for a simple choice of the single quartic coupling  $\lambda = 0$  at the SO(5)-symmetry scale  $\mu_X$ .

Figure 1 (left panel) also shows that  $g'$  and Yukawa coupling effects are *not* sufficient to yield a viable Higgs spectrum at the weak scale, starting from a SO(5)-invariant boundary condition at some high scale  $\mu_X$ . To minimally circumvent this problem, we need to include soft SO(5)-breaking effects, by assuming a non-zero value for  $\text{Re}(m_{12}^2)$  in the 2HDM potential (1.2). In the SO(5)-symmetric limit (2.8) for the scalar quartic couplings, but with  $\text{Re}(m_{12}^2) \neq 0$ , we obtain the following mass spectrum [cf. (A.5)]:

$$M_H^2 = 2\lambda_2 v^2 , \quad M_h^2 = M_a^2 = M_{h^\pm}^2 = \frac{\text{Re}(m_{12}^2)}{s_\beta c_\beta} , \tag{3.2}$$

as well as an equality between the CP-even and CP-odd mixing angles:  $\alpha = \beta$ , thus predicting an *exact* alignment for the SM-like Higgs boson  $H$ , simultaneously with an

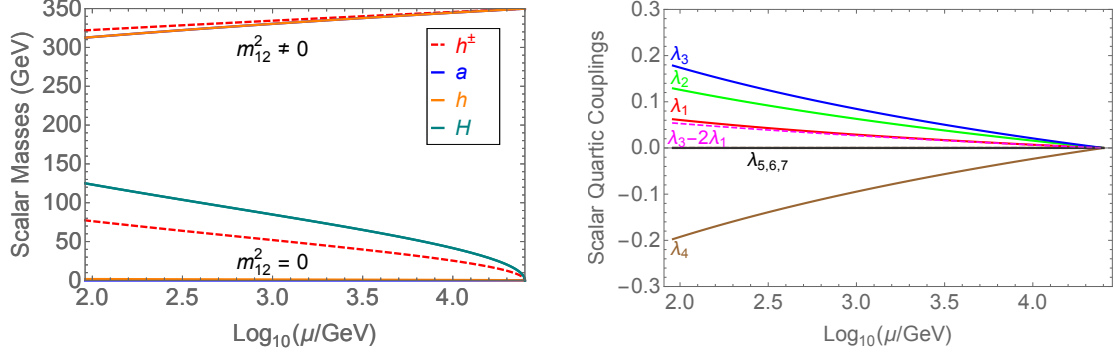


**Figure 1.** (left panel) The Higgs spectrum in the MS-2HDM without and with soft breaking effects induced by  $m_{12}^2$ . For  $m_{12}^2 = 0$ , the pseudo-Goldstone boson  $a$  remains massless at tree-level, whereas  $h$  and  $h^\pm$  receive small masses due to the  $g'$  and Yukawa coupling effects. For  $m_{12}^2 \neq 0$ , one obtains a quasi-degenerate heavy Higgs spectrum, cf. (3.2). (right panel) The RG evolution of the scalar quartic couplings under  $g'$  and Yukawa coupling effects. Here we have chosen  $\mu_X = 2.5 \times 10^4$  GeV,  $\lambda(\mu_X) = 0$  and  $\tan\beta = 50$  for illustration.

experimentally allowed heavy Higgs spectra (see left panel of Figure 1 for  $m_{12}^2 \neq 0$ ). Note that in the alignment limit, the heavy Higgs sector is exactly degenerate [cf. (3.2)] at the SO(5) symmetry-breaking scale, and at the low-energy scale, this degeneracy is mildly broken by the RG effects. Thus, we obtain a quasi-degenerate heavy Higgs spectrum in the MS-2HDM, as illustrated in Figure 1 (left panel). We emphasize that this is a unique prediction of this model, valid even in the non-decoupling limit, and can be used to distinguish it from other 2HDM scenarios.

From (3.2), we notice that the alignment limit  $\alpha = \beta$  is independent of the charged Higgs-boson mass  $M_{h^\pm}$  and the value of  $\tan\beta$ . This is achieved without *decoupling*, i.e. without the need to consider the mass hierarchy  $M_{h^\pm} \gg v$ . Hence, in this softly broken SO(5) 2HDM, we get *natural* SM alignment, *without* decoupling.<sup>6</sup> It is instructive to analyze this last point in more detail. In the general CP-conserving 2HDM, the CP-even scalar mass matrix can be written down as [42, 43]

$$\begin{aligned}
 M_S^2 &= M_a^2 \begin{pmatrix} s_\beta^2 & -s_\beta c_\beta \\ -s_\beta c_\beta & c_\beta^2 \end{pmatrix} + v^2 \begin{pmatrix} 2\lambda_1 c_\beta^2 + \lambda_5 s_\beta^2 + 2\lambda_6 s_\beta c_\beta & \lambda_{34} s_\beta c_\beta + \lambda_6 c_\beta^2 + \lambda_7 s_\beta^2 \\ \lambda_{34} s_\beta c_\beta + \lambda_6 c_\beta^2 + \lambda_7 s_\beta^2 & 2\lambda_2 s_\beta^2 + \lambda_5 c_\beta^2 + 2\lambda_7 s_\beta c_\beta \end{pmatrix} \\
 &\equiv \begin{pmatrix} c_\beta & -s_\beta \\ s_\beta & c_\beta \end{pmatrix} \widehat{M}_S^2 \begin{pmatrix} c_\beta & s_\beta \\ -s_\beta & c_\beta \end{pmatrix}, \tag{3.3}
 \end{aligned}$$

where  $M_a^2$  is given in (A.5),  $\lambda_{34} \equiv \lambda_3 + \lambda_4$ , and

$$\widehat{M}_S^2 = \begin{pmatrix} \widehat{A} & \widehat{C} \\ \widehat{C} & \widehat{B} \end{pmatrix}, \tag{3.4}$$

<sup>6</sup>Strictly speaking, there will be one-loop threshold corrections to the effective MS-2HDM potential, sourced from a non-zero  $\text{Re}(m_{12}^2)$ , which might lead to small misalignments. A simple estimate suggests that these corrections are of order  $\lambda^2/(16\pi^2)$  and can therefore be safely neglected to a good approximation.

with

$$\widehat{A} = 2v^2 \left[ c_\beta^4 \lambda_1 + s_\beta^2 c_\beta^2 \lambda_{345} + s_\beta^4 \lambda_2 + 2s_\beta c_\beta (c_\beta^2 \lambda_6 + s_\beta^2 \lambda_7) \right], \quad (3.5)$$

$$\widehat{B} = M_a^2 + \lambda_5 v^2 + 2v^2 \left[ s_\beta^2 c_\beta^2 (\lambda_1 + \lambda_2 - \lambda_{345}) - s_\beta c_\beta (c_\beta^2 - s_\beta^2) (\lambda_6 - \lambda_7) \right], \quad (3.6)$$

$$\widehat{C} = v^2 \left[ s_\beta^3 c_\beta (2\lambda_2 - \lambda_{345}) - c_\beta^3 s_\beta (2\lambda_1 - \lambda_{345}) + c_\beta^2 (1 - 4s_\beta^2) \lambda_6 + s_\beta^2 (4c_\beta^2 - 1) \lambda_7 \right]. \quad (3.7)$$

Here we have used the short-hand notation:  $\lambda_{345} \equiv \lambda_3 + \lambda_4 + \lambda_5$ . Observe that  $\widehat{M}_S^2$  in (3.3) is the respective  $2 \times 2$  CP-even mass matrix written down in the so-called Higgs eigenbasis [44–47].

Evidently, the SM alignment limit  $\alpha \rightarrow \beta$  for the CP-even scalar mixing angle  $\alpha$  is obtained, provided the off-diagonal elements of  $\widehat{M}_S^2$  in (3.4) vanish, i.e. for  $\widehat{C} = 0$  [24]. From (3.7), this yields the quartic equation

$$\lambda_7 t_\beta^4 - (2\lambda_2 - \lambda_{345}) t_\beta^3 + 3(\lambda_6 - \lambda_7) t_\beta^2 + (2\lambda_1 - \lambda_{345}) t_\beta - \lambda_6 = 0. \quad (3.8)$$

In order to satisfy (3.8) for *any* value of  $\tan \beta$ , the coefficients of the polynomial in  $\tan \beta$  must identically vanish.<sup>7</sup> Imposing this restriction, we conclude that all natural alignment solutions must satisfy the following condition:

$$\lambda_1 = \lambda_2 = \lambda_{345}/2, \quad \lambda_6 = \lambda_7 = 0. \quad (3.9)$$

In particular, for  $\lambda_6 = \lambda_7 = 0$ , (3.8) has a solution

$$\tan^2 \beta = \frac{2\lambda_1 - \lambda_{345}}{2\lambda_2 - \lambda_{345}} > 0, \quad (3.10)$$

independent of  $M_a$ . After some algebra, the simple solution (3.10) to our general alignment condition (3.8) can be shown to be equivalent to that derived in [26, 48].

In the alignment limit, the two CP-even Higgs masses are given by the diagonal elements of  $\widehat{M}_S^2$  in (3.4):

$$M_H^2 = 2v^2 (\lambda_1 c_\beta^4 + \lambda_{345} s_\beta^2 c_\beta^2 + \lambda_2 s_\beta^4) \equiv \lambda_{\text{SM}} v^2, \quad (3.11)$$

$$M_h^2 = M_a^2 + \lambda_5 v^2 + 2v^2 s_\beta^2 c_\beta^2 (\lambda_1 + \lambda_2 - \lambda_{345}). \quad (3.12)$$

On the other hand, in the limit  $M_a \gg v$ , we can use a seesaw-like approximation in (3.4) to obtain

$$M_H^2 \simeq \lambda_{\text{SM}} v^2 - \frac{v^4 s_\beta^2 c_\beta^2}{M_a^2 + \lambda_5 v^2} \left[ s_\beta^2 (2\lambda_2 - \lambda_{345}) - c_\beta^2 (2\lambda_1 - \lambda_{345}) \right]^2, \quad (3.13)$$

$$M_h^2 \simeq M_a^2 + \lambda_5 v^2 \gg v^2. \quad (3.14)$$

In (3.13) and (3.14), we have also included the possibility of decoupling via a large  $\lambda_5$  coupling [25]. For large values of  $\tan \beta$ , e.g.  $\tan \beta \gtrsim 10$ , we readily see that (3.13) reduces to  $M_H^2 \simeq 2\lambda_2 v^2$ , which again leads to a natural alignment.

<sup>7</sup>Notice that (3.8) is satisfied automatically in the SO(5) limit given in (2.8).

As noted above, in the SO(5) symmetric limit of the conformal part of the 2HDM as given by (2.8) and (3.2), the SM alignment is achieved for any value of  $\tan\beta$  [cf. (3.10)]. In addition to SO(5), one may now wonder whether there are other classified symmetries of the 2HDM that lead to natural SM alignment, *independently* of  $\tan\beta$  and  $M_a$ . According to the classification given in Table 1 of [29], we observe that, in the context of Type-II 2HDM, there are *only* two other symmetries which lead to such natural SM alignment by satisfying (3.9), viz.<sup>8</sup>

$$(i) \quad \text{O}(3) \otimes \text{O}(2) : \quad \lambda_1 = \lambda_2 = \lambda_{34}/2, \quad \lambda_5 = \lambda_6 = \lambda_7 = 0, \quad (3.15)$$

$$(ii) \quad \text{Z}_2 \otimes [\text{O}(2)]^2 : \quad \lambda_1 = \lambda_2 = \lambda_{345}/2, \quad \lambda_6 = \lambda_7 = 0. \quad (3.16)$$

Both these symmetries also require  $\mu_1^2 = \mu_2^2$  and  $m_{12}^2 = 0$ . Note that in all the three naturally aligned scenarios, cf. (2.8), (3.15) and (3.16),  $\tan\beta$  as given in (3.10) ‘consistently’ gives an *indefinite* answer 0/0. After spontaneous electroweak symmetry breaking, symmetry (i) predicts two pseudo-Goldstone bosons ( $h, a$ ), whilst symmetry (ii) predicts only one pseudo-Goldstone boson, i.e. the CP-even Higgs boson  $h$ . However, a non-zero soft SO(5)-breaking mass parameter  $m_{12}^2$  can be introduced to render the pseudo-Goldstone bosons sufficiently massive, in agreement with present experimental data, similar to the SO(5) case shown in Figure 1. Even though the 2HDM scenarios based on the symmetries (i) and (ii) may be analyzed in a similar fashion, our focus here will be on the simplest realization of the SM alignment, namely, the MS-2HDM based on the SO(5) group. Nevertheless, the results that we will be deriving in the present study are quite generic and could apply to the less symmetric cases (i) and (ii) above as well.

Before concluding this section, we would like to comment that no CP violation is possible in the MS-2HDM, be it spontaneously or explicitly, at least up to one-loop level. This is due to the fact that the Higgs potential (2.9) remains CP-invariant after the RG and one-loop threshold effects, even if a generic soft  $\text{Z}_2$ -breaking term  $\text{Im}(m_{12}^2 e^{i\xi}) \neq 0$  with an arbitrary CP-phase  $\xi$  is present. In particular, as illustrated in Figure 1 (right panel), a non-zero  $\lambda_{5,6,7}$  cannot be induced via RG effects, and this is true to any order in perturbation theory. On the other hand, one-loop threshold effects could induce non-zero  $\lambda_{5,6,7}$  of the following form:

$$\lambda_5 \sim \frac{\lambda_3^2 (m_{12}^2)^2}{16\pi^2 |m_{12}^2|^2}, \quad \lambda_6 \sim \frac{\lambda_1 \lambda_3 m_{12}^2}{16\pi^2 |m_{12}^2|}, \quad \lambda_7 \sim \frac{\lambda_2 \lambda_3 m_{12}^2}{16\pi^2 |m_{12}^2|}. \quad (3.17)$$

However, the Higgs potential still remains CP-invariant, due to the fulfillment of the following conditions [43]:

$$\text{Im}(m_{12}^4 \lambda_5^*) = \text{Im}(m_{12}^2 \lambda_6^*) = \text{Im}(m_{12}^2 \lambda_7^*) = 0. \quad (3.18)$$

Therefore, there is no ‘CP-crisis’ arising from large contributions to electric dipole moments in the MS-2HDM, unlike in the case of MSSM.

---

<sup>8</sup>In Type-I 2HDM, there exists an additional possibility of realizing an exact  $\text{Z}_2$  symmetry [33] which leads to an exact alignment, i.e. in the context of the so-called inert 2HDM [49].

## 4 Misalignment Predictions

As discussed in Section 3, a realistic Higgs spectrum can be obtained by softly breaking the maximal  $SO(5)$  symmetry of the 2HDM potential at some high scale  $\mu_X$  by considering  $\text{Re}(m_{12}^2) \neq 0$ . As a consequence, there will be some deviation from the alignment limit in the low-energy Higgs spectrum. By requiring that the mass and couplings of the SM-like Higgs boson in our MS-2HDM are consistent with the latest Higgs data from the LHC [3, 4, 50], we can derive predictions for the remaining scalar spectrum and compare them with the existing (in)direct limits on the heavy Higgs sector. Our subsequent numerical results are derived for the Type-II 2HDM scenario, but the analysis could be easily extended to other 2HDM scenarios.

For the SM-like Higgs boson mass, we will use the  $3\sigma$  allowed range from the recent CMS and ATLAS Higgs mass measurements [4, 50]:

$$M_H \in [124.1, 126.6] \text{ GeV} . \quad (4.1)$$

For the Higgs couplings to the SM vector bosons and fermions, we use the constraints in the  $(\tan \beta, \beta - \alpha)$  plane derived from a recent global fit for the Type-II 2HDM [21, 22].<sup>9</sup> For a given set of  $SO(5)$  boundary conditions  $\{\mu_X, \tan \beta(\mu_X), \lambda(\mu_X)\}$ , we thus require that the RG-evolved 2HDM parameters at the weak scale must satisfy the above constraints on the lightest CP-even Higgs boson sector. This requirement of *alignment* with the SM Higgs sector puts stringent constraints on the MS-2HDM parameter space, as shown in Figure 2. Here the solid, dashed, and dotted blue shaded regions respectively show the  $1\sigma$ ,  $2\sigma$  and  $3\sigma$  excluded regions due to misalignment of the mixing angle  $\alpha$  from its allowed range derived from the global fit. The shaded red region is theoretically inaccessible, as there is no viable solution to the RGEs in this area. We ensure that the remaining allowed (white) region satisfies the necessary theoretical constraints, i.e. positivity and vacuum stability of the Higgs potential, and perturbativity of the Higgs self-couplings [6]. From Figure 2, we find that there exists an upper limit of  $\mu_X \lesssim 10^9$  GeV on the  $SO(5)$ -breaking scale of the 2HDM potential, beyond which an ultraviolet completion of the theory must be invoked. Moreover, for  $10^5$  GeV  $\lesssim \mu_X \lesssim 10^9$  GeV, only a narrow range of  $\tan \beta$  values are allowed.

For the allowed parameter space of our MS-2HDM as shown in Figure 2, we obtain concrete predictions for the remaining Higgs spectrum. In particular, the alignment condition imposes a *lower* bound on the soft breaking parameter  $\text{Re}(m_{12}^2)$ , and hence, on the heavy Higgs spectrum. We compare this limit with the existing experimental limits on the heavy Higgs sector of the 2HDM [40], and find that the alignment limits obtained here are more stringent in a wide range of the parameter space. The most severe experimental constraint comes from the charged Higgs sector, which give significant contributions to various flavour observables, e.g.  $B \rightarrow X_s \gamma$  [51–53]. For this, we use the global fit results for the Type-II 2HDM from [21], which includes limits derived from electroweak precision data, as well as flavour constraints from  $\Delta m_{B_s}$  and  $B \rightarrow X_s \gamma$  relevant for the low  $\tan \beta$

---

<sup>9</sup>Note that in our convention, the couplings of the SM-like Higgs boson to vector bosons is proportional to  $\cos(\beta - \alpha)$  [cf. (A.8)]. Hence, the natural alignment limit is obtained for  $\alpha = \beta$ , and *not* for  $\alpha = \beta - \pi/2$ , as conventionally used in literature.

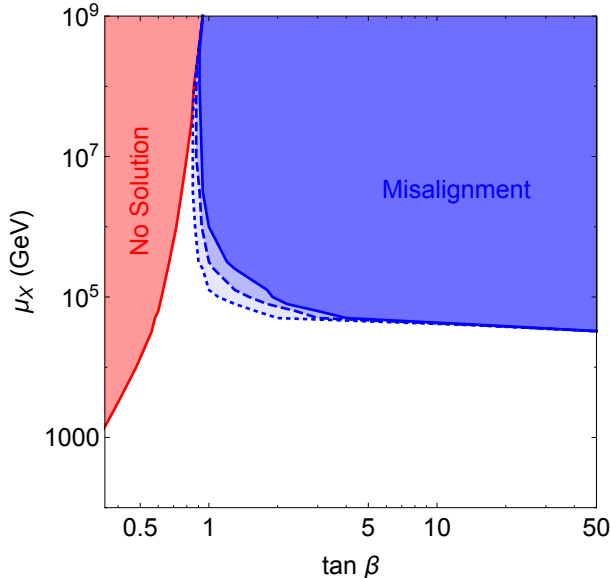


**Figure 2.** Alignment constraints in the  $(\tan\beta, \mu_X)$ -plane of the maximally symmetric Type-II 2HDM. The blue shaded regions show the  $1\sigma$  (dotted),  $2\sigma$  (dashed) and  $3\sigma$  (solid) exclusion regions from the alignment condition. The red shaded region is theoretically excluded in this model.

region. The comparison of the existing limit on the charged Higgs-boson mass as a function of  $\tan\beta$  with our predicted limits from the alignment condition for a typical value of the boundary scale  $\mu_X = 3 \times 10^4$  GeV is shown in Figure 3. It is clear that the alignment limits are stronger than the indirect limits, except in the very small and very large  $\tan\beta$  regimes. For  $\tan\beta \lesssim 1$  region, the indirect limit obtained from the  $Z \rightarrow b\bar{b}$  precision observable becomes the strictest [21, 54]. Similarly, for the large  $\tan\beta \gtrsim 30$  case, the alignment limit can be easily obtained [cf. (3.7)] without requiring a large soft-breaking parameter  $m_{12}^2$ , and therefore, the lower limit on the charged Higgs mass derived from the misalignment condition becomes somewhat weaker in this regime.

From Figure 2, it should be noted that for  $\mu_X \gtrsim 10^5$  GeV, phenomenologically acceptable alignment is not possible in the MS-2HDM for large  $\tan\beta$  and large  $m_{12}^2$ , while keeping the lightest CP-even Higgs boson within the experimentally allowed range (4.1) and maintaining vacuum stability up to the scale  $\mu_X$ . Therefore,  $\mu_X \gtrsim 10^5$  GeV also leads to an *upper* bound on the charged Higgs-boson mass  $M_{h^\pm}$  from the misalignment condition, depending on  $\tan\beta$ . This is illustrated in Figure 4 for  $\mu_X = 10^5$  GeV. Here the green shaded regions show the  $1\sigma$  (dotted),  $2\sigma$  (dashed) and  $3\sigma$  (solid) *allowed* regions, whereas the corresponding red shaded regions are the experimentally exclusion regions at  $1\sigma$  (dotted),  $2\sigma$  (dashed) and  $3\sigma$  (solid). On the other hand, for  $\mu_X \lesssim 10^5$  GeV, a phenomenologically acceptable aligned solution with an arbitrarily large  $m_{12}^2$  is allowed for any value of  $\tan\beta$  [cf. Figure 2], and hence in this case, there exists only a lower limit on  $M_{h^\pm}$ , as shown by the blue shaded (exclusion) regions in Figure 3.

Similar alignment constraints are obtained for the heavy neutral pseudo-Goldstone bosons  $h$  and  $a$ , which are predicted to be quasi-degenerate with the charged Higgs boson

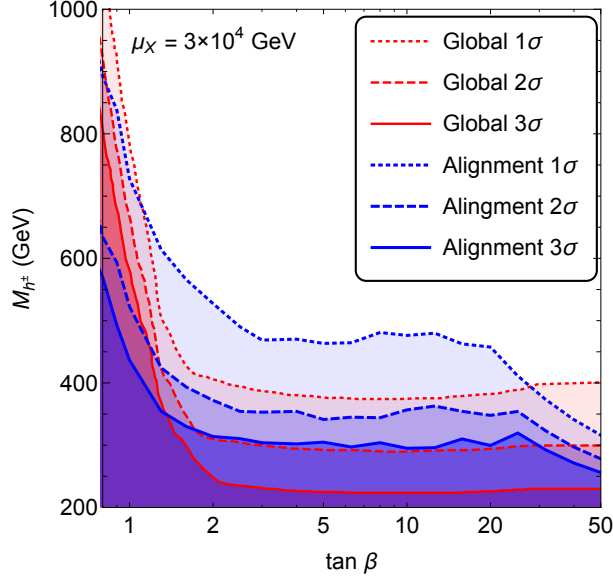


**Figure 3.** The  $1\sigma$  (dotted),  $2\sigma$  (dashed) and  $3\sigma$  (solid) lower limits on the charged Higgs mass obtained from the alignment condition (blue lines) in the maximally symmetric Type-II 2HDM with  $\mu_X = 3 \times 10^4$  GeV. For comparison, the corresponding lower limits from a global fit are also shown (red lines).

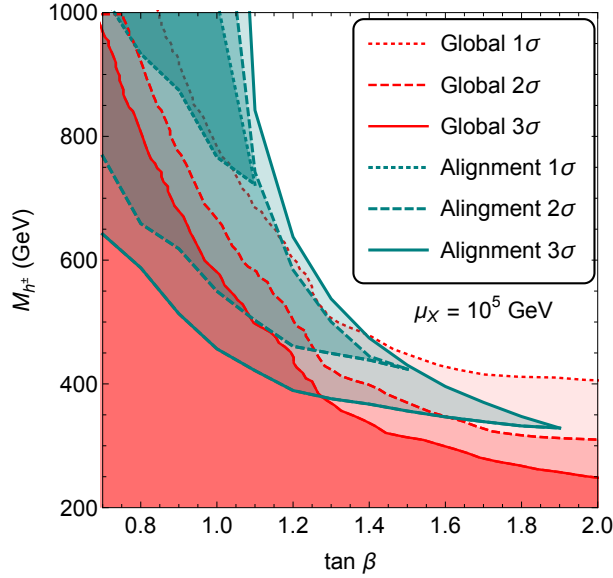


**Figure 4.** Alignment limits on the charged Higgs mass  $M_{h^\pm}$  in the maximally symmetric Type-II 2HDM with  $\mu_X = 10^5$  GeV. The dark green regions show the  $1\sigma$  (dotted),  $2\sigma$  (dashed) and  $3\sigma$  (solid) regions *allowed* by alignment constraints in the model. The existing lower limits from a global fit are also shown (red lines) for comparison.

$h^\pm$  in the MS-2HDM [cf. (3.2)]. The current experimental lower limits on the heavy neutral Higgs sector [40] are much weaker than the alignment constraints in this case. Thus, the

MS-2HDM scenario provides a natural reason for the absence of a heavy Higgs signal below the top-quark threshold, and this has important consequences for the non-standard Higgs searches in the run-II phase of the LHC, as discussed in the following section.

## 5 Collider Signals

In the alignment limit, the couplings of the lightest CP-even Higgs boson are exactly similar to the SM Higgs couplings, while the heavy CP-even Higgs boson preferentially couples to fermions (see Appendix A). Therefore, two of the relevant Higgs production mechanisms at the LHC, namely, the vector boson fusion and Higgstrahlung processes are suppressed for the gaugephobic heavy neutral Higgs sector. As a consequence, the only relevant production channels to probe the neutral Higgs sector of the MS-2HDM are the gluon-gluon fusion and  $t\bar{t}h$  ( $b\bar{b}h$ ) associated production mechanisms at low (high)  $\tan\beta$ . For the charged Higgs sector of the MS-2HDM, the dominant production mode is the associated production process:  $gg \rightarrow \bar{t}bh^+ + t\bar{b}h^-$ , irrespective of  $\tan\beta$ .

### 5.1 Branching Fractions

For our collider analysis, we calculate all the branching ratios of the heavy Higgs sector in the MS-2HDM as a function of their masses using the public C++ code 2HDMC [55]. The results for  $\tan\beta = 2$  and with SO(5)-symmetric boundary conditions at  $\mu_X = 3 \times 10^4$  GeV are shown in Figure 5 for illustration. It is clear that for the heavy neutral Higgs bosons, the  $t\bar{t}$  decay mode is the dominant one over most of the MS-2HDM parameter space. However, this is true only for low  $\tan\beta \lesssim 5$ , since as we go to higher  $\tan\beta$  values, the  $b\bar{b}$  decay mode becomes dominant, with a sub-dominant contribution from  $\tau^+\tau^-$ , whereas the  $t\bar{t}$  mode gets Yukawa suppressed. This is illustrated in Figure 6, where we compare  $\text{BR}(h \rightarrow t\bar{t})$ ,  $\text{BR}(h \rightarrow b\bar{b})$  and  $\text{BR}(h \rightarrow \tau^+\tau^-)$  for three representative values of  $\tan\beta = 2$  (solid), 5 (dashed) and 10 (dotted). For the charged Higgs boson  $h^{+(-)}$ , the  $t\bar{b}(\bar{t}b)$  mode is the dominant one over the entire parameter space, as shown in Figure 5 for  $\tan\beta = 2$ , and this is true even for larger  $\tan\beta$ .

### 5.2 Charged Higgs Signal

The detection of a charged Higgs boson will be an unequivocal evidence for a beyond SM Higgs sector, and in particular, a ‘smoking gun’ signal for a 2HDM. For  $M_{h^\pm} < M_t$ , i.e. below the top-quark threshold, stringent collider limits have been set on its production directly through top quark decays  $t \rightarrow h^+b$ , followed by  $h^+$  decays to  $\tau^+\nu_\tau$  [56, 57],  $\tau^++$  jets [58] and  $c\bar{s}$  [59, 60]. For charged Higgs boson masses above the top-quark threshold, the  $h^+ \rightarrow t\bar{b}$  decay channel opens up, and quickly becomes the dominant channel. In fact, in the Type-II 2HDM, the  $h^+t\bar{b}$  coupling (A.14) implies that for  $M_{h^+} > M_t + M_b$ , the branching fraction of  $h^+ \rightarrow t\bar{b}$  is almost 100% (cf. Figure 5), independent of  $\tan\beta$ . This leads to mostly  $t\bar{b}\bar{b}$  final states at the LHC via

$$gg \rightarrow \bar{t}bh^+ + t\bar{b}h^- \rightarrow t\bar{t}\bar{b}\bar{b}. \quad (5.1)$$

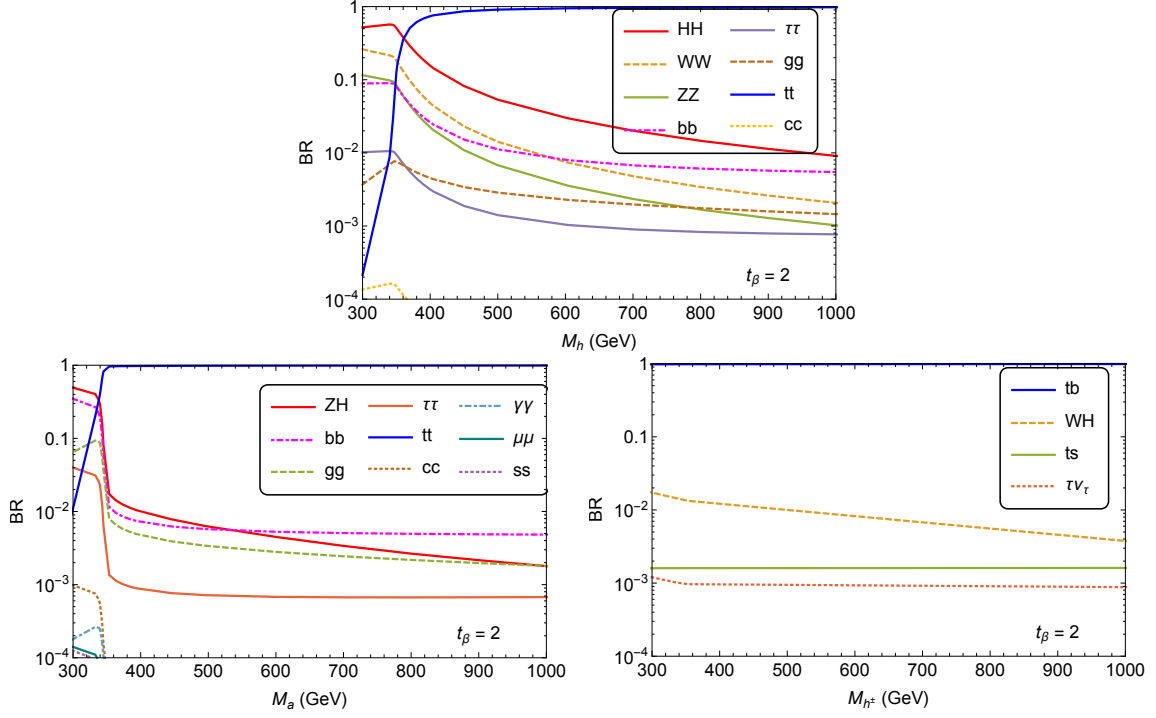


**Figure 5.** The decay branching ratios of the heavy Higgs bosons in the maximally symmetric Type-II 2HDM for low  $\tan\beta$ .

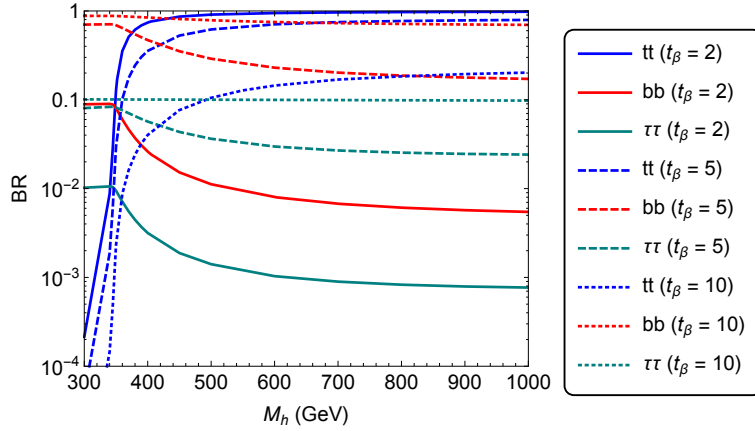


**Figure 6.** Comparison of  $\text{BR}(h \rightarrow t\bar{t})$ ,  $\text{BR}(h \rightarrow b\bar{b})$  and  $\text{BR}(h \rightarrow \tau^+\tau^-)$  for different values of  $\tan\beta$  in the maximally symmetric Type-II 2HDM.

The experimental observation of this channel is challenging due to large QCD backgrounds and the non-trivial event topology, involving at least four  $b$ -jets [61]. Nevertheless, we should emphasize here that (5.1) is the most promising channel for the charged Higgs signal in the MS-2HDM, because other interesting possibilities, such as  $h^\pm \rightarrow aW^\pm, hW^\pm$  [62], are not open in this scenario due to the kinematical constraints imposed by the quasi-degeneracy of the heavy Higgs sector [cf. (3.2) and Figure 1 (left panel)].

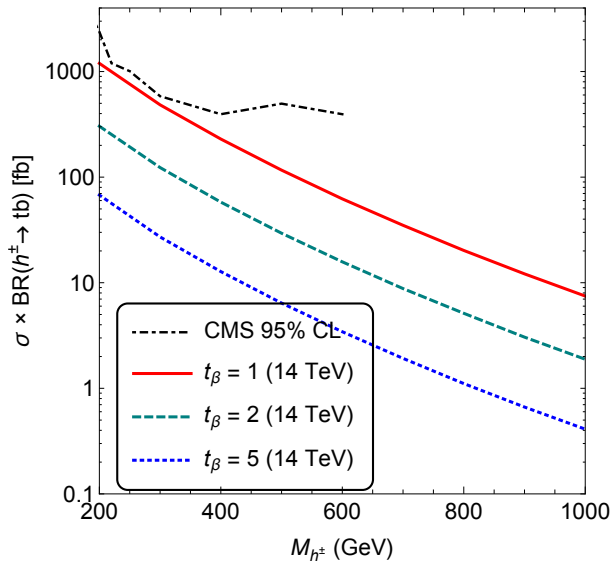


**Figure 7.** Predictions for the cross section of the process (5.1) in the Type-II MS-2HDM at  $\sqrt{s} = 14$  TeV LHC for various values of  $\tan\beta$ . For comparison, we have also shown the current 95% CL CMS upper limit from the  $\sqrt{s} = 8$  TeV data [63].

A recent CMS study [63] has presented for the first time a realistic analysis of the process (5.1), with the following decay chain:

$$gg \rightarrow h^\pm tb \rightarrow (\ell\nu_\ell bb)(\ell'\nu_{\ell'}b)b \quad (5.2)$$

( $\ell, \ell'$  beings electrons or muons). Using the  $\sqrt{s} = 8$  TeV LHC data, they have derived 95% CL upper limits on the production cross section  $\sigma(gg \rightarrow h^\pm tb)$  times the branching ratio  $\text{BR}(h^\pm \rightarrow tb)$  as a function of the charged Higgs mass, as shown in Figure 7. In the same Figure, we show the corresponding predictions at  $\sqrt{s} = 14$  TeV LHC in the Type-II MS-2HDM for some representative values of  $\tan\beta$ . The cross section predictions were obtained at leading order (LO) by implementing the 2HDM in `MadGraph5` [64] and using the `NNPDF2.3` PDF sets [65].<sup>10</sup> A comparison of these cross sections with the CMS limit suggests that the run-II phase of the LHC might be able to probe a portion of the MS-2HDM parameter space using the process (5.1).

In order to make a rough estimate of the  $\sqrt{s} = 14$  TeV LHC sensitivity to the charged Higgs signal (5.1) in the MS-2HDM, we perform a parton level simulation of the signal and background events using `MadGraph5_aMC@NLO` [64]. For the event reconstruction, we use some basic selection cuts on the transverse momentum, pseudo-rapidity and dilepton invariant mass, following the recent CMS analysis [63]:

$$\begin{aligned} p_T^\ell &> 20 \text{ GeV}, & |\eta^\ell| &< 2.5, & \Delta R^{\ell\ell} &> 0.4, \\ M_{\ell\ell} &> 12 \text{ GeV}, & |M_{\ell\ell} - M_Z| &> 10 \text{ GeV}, \\ p_T^j &> 30 \text{ GeV}, & |\eta^j| &< 2.4, & \cancel{E}_T &> 40 \text{ GeV}. \end{aligned} \quad (5.3)$$

<sup>10</sup>For an updated and improved next-to-leading order (NLO) calculation, see [66].

Jets are reconstructed using the anti- $k_T$  clustering algorithm [67] with a distance parameter of 0.5. Since four  $b$ -jets are expected in the final state, at least two  $b$ -tagged jets are required in the signal events, and we assume the  $b$ -tagging efficiency for each of them to be 70%.

The inclusive SM cross section for  $pp \rightarrow t\bar{t}b\bar{b} + X$  is  $\sim 18$  pb at NLO, with roughly 30% uncertainty due to higher order QCD corrections [68]. Most of the QCD background for the  $4b + 2\ell + \cancel{E}_T$  final state given by (5.2) can be reduced significantly by reconstructing at least one top-quark. As we will show below, the remaining irreducible background due to SM  $t\bar{t}b\bar{b}$  production can be suppressed with respect to the signal by reconstructing the charged Higgs boson mass, once a valid signal region is defined, e.g. in terms of an observed excess of events at the LHC in future. For the semi-leptonic decay mode of top-quarks as in (5.2), one cannot directly use an invariant mass observable to infer  $M_{h^\pm}$ , as both the neutrinos in the final state give rise to missing momentum. A useful quantity in this case is the  $M_{T2}$  variable, also known as the ‘stransverse mass’ [69], defined as

$$M_{T2} = \min_{\{\mathbf{p}_{T_a} + \mathbf{p}_{T_b} = \mathbf{p}_T\}} \left[ \max \{m_{T_a}, m_{T_b}\} \right], \quad (5.4)$$

where  $\{a\}, \{b\}$  stand for the two sets of particles in the final state, each containing a neutrino with part of the missing transverse momentum ( $\mathbf{p}_{T_{a,b}}$ ). Minimization over all possible sums of these two momenta gives the observed missing transverse momentum  $\mathbf{p}_T$ , whose magnitude is the same as  $\cancel{E}_T$  in our specific case. In (5.4),  $m_{T_i}$  (with  $i = a, b$ ) is the usual transverse mass variable for the system  $\{i\}$ , defined as

$$m_{T_i}^2 = \left( \sum_{\text{visible}} E_{T_i} + \cancel{E}_{T_i} \right)^2 - \left( \sum_{\text{visible}} \mathbf{p}_{T_i} + \mathbf{p}_{T_i} \right)^2. \quad (5.5)$$

For the correct combination of the final state particles in (5.2), i.e. for  $\{a\} = (\ell\nu_\ell b\bar{b})$  and  $\{b\} = (\ell'\nu_{\ell'} b\bar{b})$  in (5.4), the maximum value of  $M_{T2}$  represents the charged Higgs boson mass, with the  $M_{T2}$  distribution smoothly dropping to zero at this point. This is illustrated in Figure 8 (left panel) for a typical choice of  $M_{h^\pm} = 300$  GeV. For comparison, we also show the  $M_{T2}$  distribution for the SM background, which obviously does not have a sharp endpoint. Thus, for a given hypothesized signal region defined in terms of an excess due to  $M_{h^\pm}$ , we may impose an additional cut on  $M_{T2} \leq M_{h^\pm}$  to enhance the signal (5.2) over the irreducible SM background.

Apart from the decay chain (5.2) as considered in the CMS analysis [63], we also examine another decay chain involving hadronic decay modes of the secondary top-quark from the charged Higgs decay, i.e.

$$gg \rightarrow h^\pm tb \rightarrow (jjbb)(\ell\nu_\ell b)b. \quad (5.6)$$

In this case, the charged Higgs boson mass can be reconstructed using the invariant mass  $M_{jjbb}$  for the correct combination of the  $b$ -quark jets. This is illustrated in Figure 8 (right panel) for  $M_{h^\pm} = 300$  GeV, along with the expected SM background. Thus, for the decay chain (5.6), one can use an invariant mass cut of  $M_{jjbb}$  around  $M_{h^\pm}$  to observe the signal over the irreducible SM background. Note that the hadronic mode (5.6) has a larger

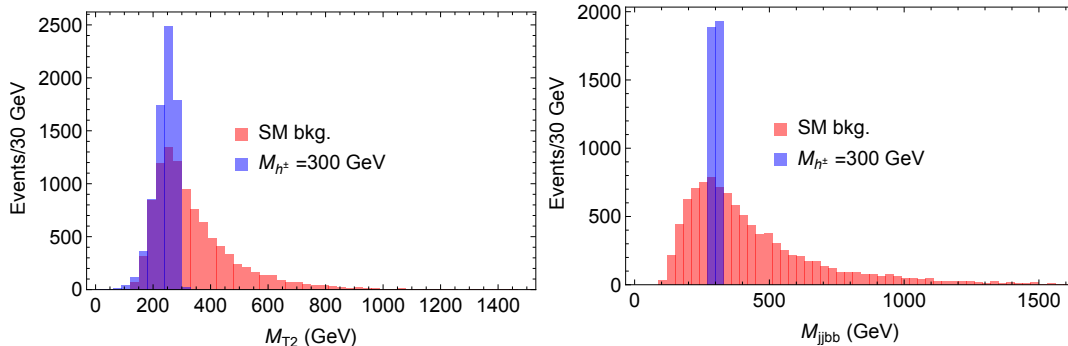


**Figure 8.** An illustration of the charged Higgs boson mass reconstruction using the  $M_{T2}$  (left panel) and invariant mass (right panel) observables. The irreducible SM background distribution is also shown for comparison.

branching ratio, although from the experimental point of view, one has to deal with the uncertainties in the jet energy measurements, combinatorics and the resulting uncertainties in the invariant mass reconstruction of multiparticle final states.

Thus, in principle, we can obtain an observable charged Higgs signal in the MS-2HDM above the irreducible SM background by using one of the methods shown in Figure 8 to reconstruct efficiently the charged Higgs boson mass. Assuming this, we present an estimate of the signal to background ratio for the charged Higgs signal given by (5.1) at  $\sqrt{s} = 14$  TeV LHC with  $300 \text{ fb}^{-1}$  for some typical values of  $\tan\beta$  in Figure 9. Since the mass of the charged Higgs boson is a priori unknown, we vary the charged Higgs mass, and for each value of  $M_{h^\pm}$ , we assume that it can be reconstructed around its actual value within 30 GeV uncertainty.<sup>11</sup> We believe such a mass resolution is feasible experimentally, given the fact that the top-quark mass resolution is of order of 1 GeV in both leptonic and hadronic channels [70]. From Figure 9, we see that the  $t\bar{t}b\bar{b}$  channel (5.1) is effective for charged Higgs searches at the LHC for low  $\tan\beta$  values. Note that the production cross section  $\sigma(gg \rightarrow \bar{t}bh^+)$  decreases rapidly with increasing  $\tan\beta$  due to the Yukawa suppression [cf. (A.14)], even though  $\text{BR}(h^+ \rightarrow \bar{t}b)$  remains close to 100%.

### 5.3 Heavy Neutral Higgs Signal

Since the heavy CP-even Higgs boson in the MS-2HDM is gaugephobic, most of the existing collider limits derived using the decay modes  $h \rightarrow WW$  [71, 72] and  $h \rightarrow ZZ$  [73] do not apply in this case. The only existing searches relevant to the heavy CP-even sector of the MS-2HDM scenario are those based on  $gg \rightarrow h \rightarrow \tau^+\tau^-$  and  $gg \rightarrow b\bar{b}h \rightarrow b\bar{b}\tau^+\tau^-$  [74, 75]. However, due to the relatively small branching ratio of  $h \rightarrow \tau^+\tau^-$ , the model-independent upper limits derived in [74, 75] are easily satisfied for the heavy Higgs spectrum presented here. Similarly, the  $h \rightarrow \gamma\gamma$  branching ratio in the MS-2HDM is  $\sim 10^2 - 10^3$  times smaller than that for the SM Higgs boson; therefore, the cross section limits derived from the  $\gamma\gamma$

<sup>11</sup>The uncertainty chosen here is always larger than the width of the charged Higgs boson  $\Gamma_{h^\pm}$  in the entire mass range shown in Figure 9. For instance, for  $\tan\beta = 2$ ,  $\Gamma_{h^\pm} = 1.9$  GeV at  $M_{h^\pm} = 300$  GeV and  $\Gamma_{h^\pm} = 22$  GeV at  $M_{h^\pm} = 2$  TeV.

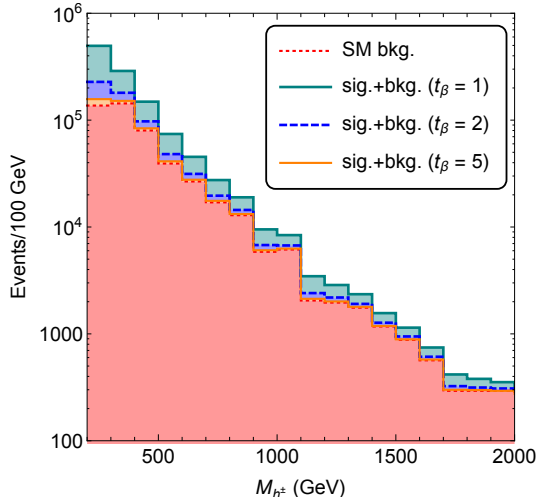


**Figure 9.** Predicted number of events for the  $t\bar{t}b\bar{b}$  signal from the charged pseudo-Goldstone boson in the MS-2HDM at  $\sqrt{s} = 14$  TeV LHC with  $300 \text{ fb}^{-1}$  integrated luminosity. The results are shown for three different values of  $\tan\beta = 1$  (green solid), 2 (blue dashed) and 5 (orange solid). The irreducible SM background (red dotted) is controlled by assuming an efficient mass reconstruction technique, as described in the text.

channel [76, 77] are also easily satisfied. So far there have been no direct searches for heavy neutral Higgs bosons involving  $t\bar{t}$  and/or  $b\bar{b}$  final states, mainly due to the challenges associated with uncertainties in the jet energy scales and the combinatorics arising from complicated multiparticle final states in a busy QCD environment. Nevertheless, these channels become pronounced in the MS-2HDM scenario, and hence, we will make here a preliminary attempt to study them.

It is worth mentioning here that the Higgs pair production process  $pp \rightarrow h \rightarrow HH$  (see e.g. [78]) is another interesting possibility. However, as shown in (A.12), the  $h \rightarrow HH$  decay mode should also vanish in the exact alignment limit  $\alpha \rightarrow \beta$ , just like the  $h \rightarrow VV$  decay modes. Therefore, the LHC limits derived using the  $h \rightarrow HH$  channel [79, 80] are applicable only below the top threshold  $M_h \leq 2M_t$  in the MS-2HDM (cf. Figure 5). On the other hand, the lower limits on the heavy Higgs sector, as derived in Section 4 (e.g. Figures 3 and 4) strongly suggest a mass spectrum above the  $t\bar{t}$  threshold, where the  $h \rightarrow HH$  branching fraction drops orders of magnitude below that of  $h \rightarrow t\bar{t}$  ( $b\bar{b}$ ) at low (high)  $\tan\beta$ .

In light of the above discussion, we propose a new search channel for the heavy neutral Higgs boson in the MS-2HDM via the  $t\bar{t}t\bar{t}$  final state:

$$gg \rightarrow t\bar{t}h \rightarrow t\bar{t}t\bar{t}. \quad (5.7)$$

Such four top final states have been proposed before in the context of other exotic searches at the LHC, e.g. composite top [81–83], low-scale extra-dimensions [84, 85] and SUSY with light stops and gluinos [86]. However, their relevance for heavy Higgs searches have not been explored so far. We note here that the existing 95% CL experimental upper limit on

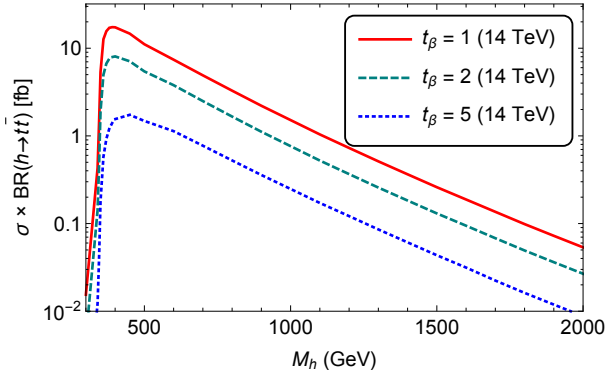


**Figure 10.** Predictions for the cross section of the process (5.7) in the Type-II MS-2HDM at  $\sqrt{s} = 14$  TeV LHC for various values of  $\tan\beta$ .

the four top production cross section is 59 fb from ATLAS [87] and 32 fb from CMS [88], whereas the SM prediction for the inclusive cross section of the process  $pp \rightarrow t\bar{t}t\bar{t} + X$  is about 10-15 fb [89].

To get a rough estimate of the signal to background ratio for our new four-top signal, we perform a parton-level simulation of the signal and background events at LO in QCD using MadGraph5\_aMC@NLO [64] with NNPDF2.3 PDF sets [65]. For the inclusive SM cross section for the four-top final state at  $\sqrt{s} = 14$  TeV LHC, we obtain 11.85 fb, whereas our proposed four-top signal cross sections are found to be comparable or smaller depending on  $M_h$  and  $\tan\beta$ , as shown in Figure 10. However, since we expect one of the  $t\bar{t}$  pairs coming from an on-shell  $h$  decay to have an invariant mass around  $M_h$ , we can use this information to significantly boost the signal over the irreducible SM background. Note that all the predicted cross sections shown in Figure 10 are well below the current experimental upper bound [88].

Depending on the  $W$  decay mode from  $t \rightarrow Wb$ , there are 35 final states for four top decays. According to a recent ATLAS analysis [90], the experimentally favoured channel is the semi-leptonic/hadronic final state with two same-sign isolated leptons. Although the branching fraction for this topology (4.19%) is smaller than most of the other channels, the presence of two same-sign leptons in the final state allows us to reduce the large QCD background substantially, including that due to the SM production of  $t\bar{t}b\bar{b} + \text{jets}$ .<sup>12</sup> Therefore, we will only consider the following decay chain in our preliminary analysis:

$$gg \rightarrow t\bar{t}h \rightarrow (t\bar{t})(t\bar{t}) \rightarrow \left( (\ell^\pm \nu_\ell b)(j\bar{j}b) \right) \left( (\ell'^\pm \nu_{\ell'} b)(j\bar{j}b) \right). \quad (5.8)$$

For event reconstruction, we will use the same selection cuts as in (5.3), and in addition, following [90], we require the scalar sum of the  $p_T$  of all leptons and jets (defined as  $H_T$ ) to exceed 350 GeV.

As in the charged Higgs boson case [cf. (5.2)], the heavy Higgs mass can be reconstructed from the signal given by (5.8) using the  $M_{T2}$  endpoint technique. The correct combination of visible final states in (5.8) will lead to a smooth drop at  $M_h$  in the  $M_{T2}$

<sup>12</sup>For a detailed analysis of the reducible and irreducible four top background, see [90].

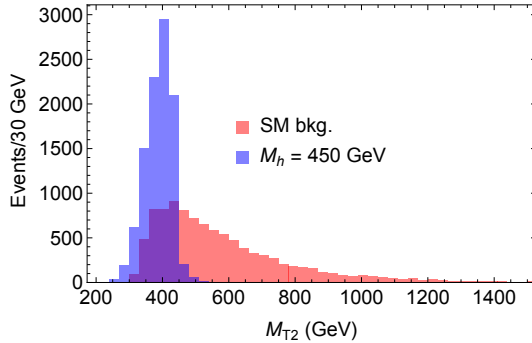


**Figure 11.** An illustration of the heavy CP-even Higgs boson mass reconstruction using  $M_{T2}$  observable. The irreducible SM background distribution is also shown for comparison.

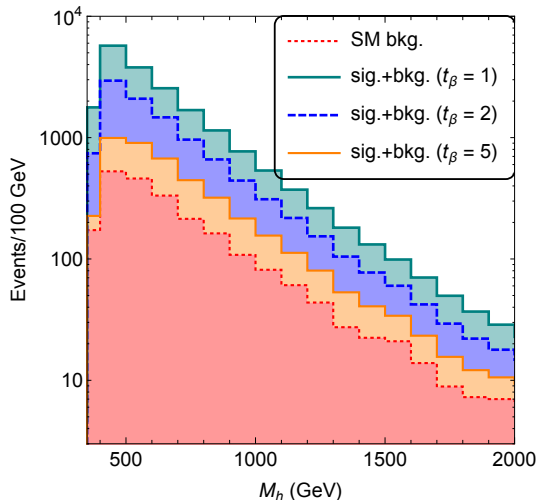


**Figure 12.** Predicted number of events for the  $t\bar{t}t\bar{t}$  signal from the neutral pseudo-Goldstone boson in the MS-2HDM at  $\sqrt{s} = 14$  TeV LHC with  $300 \text{ fb}^{-1}$  integrated luminosity. The results are shown for three different values of  $\tan\beta = 1$  (green solid), 2 (blue dashed) and 5 (orange solid). The SM background (red dotted) is controlled by assuming an efficient mass reconstruction technique, as outlined in the text.

distribution, as illustrated in Figure 11 for a typical choice of  $M_h = 450$  GeV. As shown in the same figure, the SM background does not exhibit such a feature, and hence, an additional selection cut on  $M_{T2} \leq M_h$  can be used to enhance the signal to background ratio in the signal region.

Our simulation results for the predicted number of signal and background events for the process (5.8) at  $\sqrt{s} = 14$  TeV LHC with  $300 \text{ fb}^{-1}$  luminosity are shown in Figure 12. The signal events are shown for three representative values of  $\tan\beta$ . Here we vary the a priori unknown heavy Higgs mass, and for each value of  $M_h$ , we assume that it can be reconstructed around its actual value within 30 GeV uncertainty, which should be feasible experimentally, as argued at the end of Subsection 5.2. From this preliminary analysis, we find that the  $t\bar{t}t\bar{t}$  channel provides the most promising collider signal to probe the heavy Higgs sector in the MS-2HDM at low values of  $\tan\beta \lesssim 5$ .

The above analysis is also applicable for the CP-odd Higgs boson  $a$ , which has similar production cross sections and  $t\bar{t}$  branching fractions as the CP-even Higgs  $h$ . However, the  $t\bar{t}h(a)$  production cross section as well as the  $h(a) \rightarrow t\bar{t}$  branching ratio decreases with increasing  $\tan\beta$ . This is due to the fact that the  $ht\bar{t}$  coupling in the alignment limit is  $\cos\alpha/\sin\beta \sim \cot\beta$ , which is same as the  $at\bar{t}$  coupling [cf. (A.13)]. Thus, the high  $\tan\beta$  region of the MS-2HDM cannot be searched via the  $t\bar{t}t\bar{t}$  channel proposed above, and one needs to consider the channels involving down-sector Yukawa couplings, e.g.  $b\bar{b}b\bar{b}$  and  $b\bar{b}\tau^+\tau^-$ , which are very challenging in the LHC environment [61]. For instance, the SM  $b\bar{b}b\bar{b}$  cross section at  $\sqrt{s} = 14$  TeV LHC is about 140 pb at NLO [91], whereas the  $pp \rightarrow b\bar{b}h \rightarrow b\bar{b}b\bar{b}$  signal cross section for  $M_h = 300$  GeV and  $\tan\beta = 10$  is only about 0.3 pb at NLO, as estimated using the public FORTRAN code `SusHi` [92]. In practice, one would require a sophisticated jet substructure technique [93, 94] to disentangle such a tiny signal from the huge QCD background. It is also worth commenting here that the simpler process  $pp \rightarrow h \rightarrow t\bar{t}$  ( $b\bar{b}$ ) at low (high)  $\tan\beta$  similarly suffers from a huge SM  $t\bar{t}$  ( $b\bar{b}$ ) QCD background, even after imposing an  $M_{t\bar{t}}$  ( $b\bar{b}$ ) cut.

Before concluding this section, we should clarify that although we were able to obtain a sizeable signal-to-background ratio in the low  $\tan\beta$  regime for the signals (5.2), (5.6) and (5.8) using efficient mass reconstruction techniques in the signal region, as described in Subsections 5.2 and 5.3 above, these results are valid only at the parton level. In a realistic detector environment, the sharp features of the signal shown in Figures 8 and 11 may not survive, and therefore, the signal-to-background ratio might get somewhat reduced than that shown here. However, a detailed realistic detector-level analysis of these signals in our MS-2HDM scenario, including realistic top reconstruction efficiencies and smearing effects, is beyond the scope and main focus of this article, and is being pursued in a separate dedicated study.

## 6 Conclusions

We have analyzed the symmetries of the 2HDM scalar potential to naturally justify the so-called SM alignment limit, independently of the heavy Higgs spectrum and the value of  $\tan\beta$ . We show that in the Type-II 2HDM, there exist *only* three different symmetry realizations, cf. (2.8), (3.15) and (3.16), which could lead to a natural alignment by satisfying (3.8) for *any* value of  $\tan\beta$ . In the context of the Maximally Symmetric Two Higgs Doublet Model based on the SO(5) group, we demonstrate how small deviations from this alignment limit are naturally induced by RG effects due to the hypercharge gauge coupling  $g'$  and third generation Yukawa couplings, which also break the custodial symmetry of the theory. In addition, a non-zero soft SO(5)-breaking mass parameter is required to yield a viable Higgs spectrum consistent with the existing experimental constraints. Employing the current Higgs signal strength data from the LHC, which disfavour large deviations from the alignment limit, we derive important constraints on the 2HDM parameter space. In particular, we predict lower limits on the heavy Higgs spectrum, which prevail the present limits in a wide range of parameter space. Depending on the scale where the maximal symmetry could be realized in nature, we also obtain an upper limit on the heavy Higgs

masses in certain cases, which could be completely probed during the run-II phase of the LHC. Finally, we propose a new collider signal with four top quarks in the final state, which can become a valuable observational tool to directly probe the heavy Higgs sector of the 2HDM in the alignment limit for low values of  $\tan\beta$ . It would be interesting to investigate how this tool could be applied to supersymmetric theories in the alignment limit.

## Acknowledgments

A.P. thanks Celso Nishi for a clarifying remark that led us to include the fourth footnote in this article. P.S.B.D. thanks Otto Eberhardt and Martin Wiebusch for helpful discussions regarding their global fit results in [21, 22]. We also thank Rohini Godbole, Romain Madar, Yvonne Peters and José Santiago for valuable comments on the four top analysis. The work of P.S.B.D. and A.P. is supported by the Lancaster-Manchester-Sheffield Consortium for Fundamental Physics under STFC grant ST/J000418/1.

## A Higgs Spectrum and Couplings in a General 2HDM

Here we will restrict our discussion to 2HDM potentials realizing CP-conserving vacua. In this case, the minimization of a CP-conserving 2HDM potential (1.2) yields the following real non-negative vacuum expectation values (VEVs):

$$\langle\Phi_1\rangle = \frac{1}{\sqrt{2}} \begin{pmatrix} 0 \\ v_1 \end{pmatrix}, \quad \langle\Phi_2\rangle = \frac{1}{\sqrt{2}} \begin{pmatrix} 0 \\ v_2 \end{pmatrix}, \quad (\text{A.1})$$

where  $v = \sqrt{v_1^2 + v_2^2} = 246.2$  GeV is the SM electroweak VEV and for later convenience, we define  $\tan\beta \equiv v_2/v_1$ . The two scalar doublets can be expanded in terms of eight real scalar fields as follows:

$$\Phi_j = \begin{pmatrix} \phi_j^+ \\ \frac{1}{\sqrt{2}}(v_j + \phi_j + ia_j) \end{pmatrix}, \quad (\text{A.2})$$

with  $j = 1, 2$ . After spontaneous symmetry breaking, there are three Goldstone modes ( $G^\pm, G^0$ ), which become the longitudinal components of the SM  $W^\pm$  and  $Z$  bosons. Thus, there are five remaining physical scalar mass eigenstates: two CP-even ( $h, H$ ), one CP-odd ( $a$ ) and two charged ( $h^\pm$ ) scalars. The mixing in the CP-odd and charged sectors is governed by the angle  $\beta$  defined above:

$$\begin{pmatrix} G^\pm \\ h^\pm \end{pmatrix} = \begin{pmatrix} c_\beta & s_\beta \\ -s_\beta & c_\beta \end{pmatrix} \begin{pmatrix} \phi_1^\pm \\ \phi_2^\pm \end{pmatrix}, \\ \begin{pmatrix} G^0 \\ a \end{pmatrix} = \begin{pmatrix} c_\beta & s_\beta \\ -s_\beta & c_\beta \end{pmatrix} \begin{pmatrix} a_1 \\ a_2 \end{pmatrix}, \quad (\text{A.3})$$

where  $c_\beta \equiv \cos\beta$ ,  $s_\beta \equiv \sin\beta$ . On the other hand, in the CP-even sector, we have a new mixing angle  $\alpha$ :

$$\begin{pmatrix} H \\ h \end{pmatrix} = \begin{pmatrix} c_\alpha & s_\alpha \\ -s_\alpha & c_\alpha \end{pmatrix} \begin{pmatrix} \phi_1 \\ \phi_2 \end{pmatrix}. \quad (\text{A.4})$$

The corresponding physical mass eigenvalues are given by [42, 43]

$$\begin{aligned}
M_{h^\pm}^2 &= \frac{m_{12}^2}{s_\beta c_\beta} - \frac{v^2}{2} (\lambda_4 + \lambda_5) + \frac{v^2}{2s_\beta c_\beta} (\lambda_6 c_\beta^2 + \lambda_7 s_\beta^2), \\
M_a^2 &= M_{h^\pm}^2 + \frac{v^2}{2} (\lambda_4 - \lambda_5), \\
M_H^2 &= \frac{1}{2} \left[ (A + B) - \sqrt{(A - B)^2 + 4C^2} \right], \\
M_h^2 &= \frac{1}{2} \left[ (A + B) + \sqrt{(A - B)^2 + 4C^2} \right],
\end{aligned} \tag{A.5}$$

where we have defined  $\tan 2\alpha = 2C/(A - B)$ , and

$$\begin{aligned}
A &= M_a^2 s_\beta^2 + v^2 (2\lambda_1 c_\beta^2 + \lambda_5 s_\beta^2 + 2\lambda_6 s_\beta c_\beta), \\
B &= M_a^2 c_\beta^2 + v^2 (2\lambda_2 s_\beta^2 + \lambda_5 c_\beta^2 + 2\lambda_7 s_\beta c_\beta), \\
C &= -M_a^2 s_\beta c_\beta + v^2 (\lambda_{34} s_\beta c_\beta + \lambda_6 c_\beta^2 + \lambda_7 s_\beta^2).
\end{aligned} \tag{A.6}$$

with  $\lambda_{34} = \lambda_3 + \lambda_4$ . The SM Higgs field is given by

$$H_{\text{SM}} = \phi_1 \cos \beta + \phi_2 \sin \beta = H \cos(\beta - \alpha) + h \sin(\beta - \alpha). \tag{A.7}$$

From (A.7), the couplings of  $h$  and  $H$  to the gauge bosons ( $V = W^\pm, Z$ ) with respect to the SM Higgs couplings  $g_{H_{\text{SM}}VV}$  are given by

$$g_{hVV} = s_{\beta-\alpha}, \quad g_{HVV} = c_{\beta-\alpha}. \tag{A.8}$$

Similarly, unitarity constraints uniquely fix the other Higgs-Higgs- $V$  couplings [5]:

$$\begin{aligned}
g_{haZ} &= \frac{g}{2 \cos \theta_w} c_{\beta-\alpha}, & g_{HaZ} &= \frac{g}{2 \cos \theta_w} s_{\beta-\alpha}, \\
g_{h+hW^-} &= \frac{g}{2} c_{\beta-\alpha}, & g_{h+HW^-} &= \frac{g}{2} s_{\beta-\alpha}, & g_{ah^\pm W^\mp} &= \frac{g}{2},
\end{aligned} \tag{A.9}$$

(where  $\theta_w$  is the weak mixing angle) in order to satisfy the sum rules [95]

$$g_{haZ}^2 + g_{HaZ}^2 = \frac{1}{\cos^2 \theta_w} (g_{h+hW^-}^2 + g_{h+HW^-}^2) = \frac{1}{4M_Z^2} g_{H_{\text{SM}}ZZ}^2, \tag{A.10}$$

$$g_{h+hW^-}^2 + g_{h+HW^-}^2 = g_{ah^\pm W^\mp}^2 = \frac{1}{4M_W^2} g_{H_{\text{SM}}W^+W^-}^2. \tag{A.11}$$

For our subsequent discussion, we also write down the  $h$ - $H$ - $H$  coupling [24]:

$$\begin{aligned}
g_{hHH} &= \frac{s_{\beta-\alpha}}{4v s_\beta c_\beta} \left[ 2(M_h^2 + 2M_H^2) s_{2\alpha} - 2(M_a^2 + v^2 \lambda_5) (s_{2\beta} + 3s_{2\alpha}) \right. \\
&\quad \left. - v^2 (\lambda_6 - \lambda_7) (c_{2\beta} + 3c_{2\alpha}) - v^2 (\lambda_6 + \lambda_7) (1 + 3c_{2(\beta-\alpha)}) \right].
\end{aligned} \tag{A.12}$$

Note that the coupling  $g_{hHH}$  is proportional to  $s_{\beta-\alpha}$  and so vanishes identically in the alignment limit  $\alpha \rightarrow \beta$ .

To obtain a phenomenologically acceptable theory, we need to forbid Higgs interactions with tree-level FCNCs. This can be accomplished minimally by imposing appropriate

discrete  $Z_2$  symmetries, which will explicitly break in general the custodial symmetries of the theory. By convention, we may take  $u_R$  to couple to  $\Phi_2$ , i.e.  $h_1^u = 0$ , and then  $\Phi_1$  ( $\Phi_2$ ) to couple to  $d_R$ , with  $h_2^d = 0$  ( $h_1^d = 0$ ), in a Type-II (Type-I) realization of the 2HDM. As our interest is in the Type-II 2HDM, we only list the Yukawa couplings of the neutral scalars with respect to those of  $H_{\text{SM}}$  for this class of models [5]:

$$\begin{aligned} g_{ht\bar{t}} &= \cos\alpha/\sin\beta, & g_{hb\bar{b}} &= -\sin\alpha/\cos\beta, \\ g_{Ht\bar{t}} &= \sin\alpha/\sin\beta, & g_{Hb\bar{b}} &= \cos\alpha/\cos\beta, \\ g_{at\bar{t}} &= \cot\beta, & g_{abb} &= \tan\beta. \end{aligned} \quad (\text{A.13})$$

Finally, we also write down the coupling of the charged scalar to the third-generation quarks [5]:

$$g_{h^-t\bar{b}} = \frac{g}{2\sqrt{2}M_W} [m_t \cot\beta(1 + \gamma_5) + m_b \tan\beta(1 - \gamma_5)]. \quad (\text{A.14})$$

## B Two-loop RGEs in a General 2HDM

In this section, we present the two-loop renormalization group equations (RGEs) for the general 2HDM given by (1.2). These results were obtained using the general prescription given in [96], as implemented in the public `Mathematica` package `SARAH 4` [97].

The two-loop RGEs for the  $SU(3)_c$ ,  $SU(2)_L$  and  $U(1)_Y$  gauge couplings are respectively given by

$$\mathcal{D}g_3 = -\frac{7g_3^3}{16\pi^2} + \frac{g_3^3}{256\pi^4} \left( -26g_3^2 + \frac{9}{2}g_2^2 + \frac{11}{6}g'^2 - 2y_b^2 - 2y_t^2 \right), \quad (\text{B.1})$$

$$\mathcal{D}g_2 = -\frac{3g_2^3}{16\pi^2} + \frac{g_2^3}{256\pi^4} \left( 12g_3^2 + 8g_2^2 + 2g'^2 - \frac{3}{2}y_b^2 - \frac{3}{2}y_t^2 - \frac{1}{2}y_\tau^2 \right), \quad (\text{B.2})$$

$$\mathcal{D}g' = \frac{7g'^3}{16\pi^2} + \frac{g'^3}{256\pi^4} \left( \frac{44}{3}g_3^2 + 6g_2^2 + \frac{104}{9}g'^2 - \frac{5}{6}y_b^2 - \frac{17}{6}y_t^2 - \frac{5}{2}y_\tau^2 \right), \quad (\text{B.3})$$

where  $\mathcal{D} \equiv d/d\ln\mu$  and  $\mu$  is the usual 't-Hooft mass employed in the regularization of ultraviolet divergences in loop integrals. Note that at the one-loop level, the gauge coupling RGEs do not depend on the Yukawa and scalar couplings, whilst at two loops, they do depend on the quark and lepton Yukawa couplings, for which we have only kept the dominant third-generation contributions.

Similarly for the Yukawa RGEs, we will only consider the third-generation Yukawa couplings, such that for Type-II 2HDM, we have

$$m_t = \frac{v_2}{\sqrt{2}} h_{2,33}^u \equiv \frac{v_2}{\sqrt{2}} y_t, \quad m_{b(\tau)} = \frac{v_1}{\sqrt{2}} h_{1,33}^{d(e)} \equiv \frac{v_1}{\sqrt{2}} y_{b(\tau)}. \quad (\text{B.4})$$

With this approximation, the third-generation Yukawa coupling RGEs are given by

$$\begin{aligned} \mathcal{D}y_t &= \frac{y_t}{16\pi^2} \left( -8g_3^2 - \frac{9}{4}g_2^2 - \frac{17}{12}g'^2 + \frac{9}{2}y_t^2 + \frac{1}{2}y_b^2 \right) \\ &+ \frac{y_t}{256\pi^4} \left[ -108g_3^4 - \frac{21}{4}g_2^4 + \frac{1267}{216}g'^4 + 9g_2^2g_3^2 - \frac{3}{4}g_2^2g'^2 + \frac{19}{9}g_3^2g'^2 + 6\lambda_2^2 + \lambda_3^2 \right] \end{aligned}$$

$$\begin{aligned}
& + \lambda_3 \lambda_4 + \lambda_4^2 + \frac{3}{2}(\lambda_5^2 + \lambda_6^2 + 3\lambda_7^2) + \left( \frac{16}{3}g_3^2 + \frac{33}{16}g_2^2 - \frac{41}{144}g'^2 - 2\lambda_3 + 2\lambda_4 \right) y_b^2 \\
& + \left( 36g_3^2 + \frac{225}{16}g_2^2 + \frac{131}{16}g'^2 - 12\lambda_2 \right) y_t^2 - \frac{5}{2}y_b^4 - 12y_t^4 - \frac{5}{2}y_b^2 y_t^2 - \frac{3}{4}y_b^2 y_\tau^2 \Big], \quad (\text{B.5})
\end{aligned}$$

$$\begin{aligned}
\mathcal{D}y_b &= \frac{y_b}{16\pi^2} \left( -8g_3^2 - \frac{9}{4}g_2^2 - \frac{5}{12}g'^2 + \frac{9}{2}y_b^2 + \frac{1}{2}y_t^2 + y_\tau^2 \right) \\
& + \frac{y_b}{256\pi^4} \left[ -108g_3^4 - \frac{21}{4}g_2^4 - \frac{113}{216}g'^4 + 9g_2^2 g_3^2 - \frac{9}{4}g_2^2 g'^2 + \frac{31}{9}g_3^2 g'^2 + 6\lambda_1^2 + \lambda_3^2 \right. \\
& + \lambda_3 \lambda_4 + \lambda_4^2 + \frac{3}{2}(\lambda_5^2 + 3\lambda_6^2 + \lambda_7^2) + \left( \frac{16}{3}g_3^2 + \frac{33}{16}g_2^2 - \frac{53}{144}g'^2 - 2\lambda_3 + 2\lambda_4 \right) y_t^2 \\
& + \left( \frac{15}{8}g_2^2 + \frac{25}{8}g'^2 \right) y_\tau^2 + \left( 36g_3^2 + \frac{225}{16}g_2^2 + \frac{79}{16}g'^2 - 12\lambda_1 \right) y_b^2 \\
& \left. - 12y_b^4 - \frac{9}{4}y_\tau^4 - \frac{5}{2}y_t^4 - \frac{5}{2}y_b^2 y_t^2 - \frac{9}{4}y_b^2 y_\tau^2 \right], \quad (\text{B.6})
\end{aligned}$$

$$\begin{aligned}
\mathcal{D}y_\tau &= \frac{y_\tau}{16\pi^2} \left( -\frac{9}{4}g_2^2 - \frac{15}{4}g'^2 + 3y_b^2 + \frac{5}{2}y_\tau^2 \right) \\
& + \frac{y_\tau}{256\pi^4} \left[ -\frac{21}{4}g_2^4 + \frac{161}{8}g'^4 + \frac{9}{4}g_2^2 g'^2 + 6\lambda_1^2 + \lambda_3^2 + \lambda_3 \lambda_4 + \lambda_4^2 \right. \\
& + \frac{3}{2}(\lambda_5^2 + 3\lambda_6^2 + \lambda_7^2) + \left( 20g_3^2 + \frac{45}{8}g_2^2 + \frac{25}{24}g'^2 \right) y_b^2 \\
& \left. + \left( \frac{165}{16}g_2^2 + \frac{179}{16}g'^2 - 12\lambda_1 \right) y_\tau^2 - \frac{27}{4}y_b^4 - 3y_\tau^4 - \frac{27}{4}y_b^2 y_\tau^2 - \frac{9}{4}y_b^2 y_t^2 \right]. \quad (\text{B.7})
\end{aligned}$$

Similarly, the two-loop RGEs for the VEVs are given by

$$\begin{aligned}
\mathcal{D}v_1 &= \frac{v_1}{16\pi^2} \left[ \frac{3}{4}(3g_2^2 + g'^2) - 3y_b^2 - y_\tau^2 \right] \\
& + \frac{v_1}{256\pi^4} \left[ \frac{435}{32}g_2^4 - \frac{149}{32}g'^4 - \frac{3}{16}g_2^2 g'^2 - 6\lambda_1^2 - \lambda_3^2 - \lambda_3 \lambda_4 - \lambda_4^2 \right. \\
& - \frac{3}{2}(\lambda_5^2 + 3\lambda_6^2 + \lambda_7^2) - \left( 20g_3^2 + \frac{45}{8}g_2^2 + \frac{25}{24}g'^2 \right) y_b^2 - \left( \frac{15}{8}g_2^2 + \frac{25}{8}g'^2 \right) y_\tau^2 \\
& \left. + \frac{27}{4}y_b^4 + \frac{9}{4}y_\tau^4 + \frac{9}{4}y_b^2 y_\tau^2 \right] - \frac{3v_2}{512\pi^4} \left[ (2\lambda_1 + \lambda_{345})\lambda_6 + (2\lambda_2 + \lambda_{345})\lambda_7 \right], \quad (\text{B.8})
\end{aligned}$$

$$\begin{aligned}
\mathcal{D}v_2 &= \frac{v_2}{16\pi^2} \left[ \frac{3}{4}(3g_2^2 + g'^2) - 3y_t^2 \right] \\
& + \frac{v_2}{256\pi^4} \left[ \frac{435}{32}g_2^4 - \frac{149}{32}g'^4 - \frac{3}{16}g_2^2 g'^2 - 6\lambda_2^2 - \lambda_3^2 - \lambda_3 \lambda_4 - \lambda_4^2 \right. \\
& - \frac{3}{2}(\lambda_5^2 + \lambda_6^2 + 3\lambda_7^2) - \left( 20g_3^2 + \frac{45}{8}g_2^2 + \frac{85}{24}g'^2 \right) y_t^2 + \frac{9}{4}y_b^2 y_t^2 + \frac{27}{4}y_t^4 \Big] \\
& - \frac{3v_1}{512\pi^4} \left[ (2\lambda_1 + \lambda_{345})\lambda_6 + (2\lambda_2 + \lambda_{345})\lambda_7 \right]. \quad (\text{B.9})
\end{aligned}$$

The two-loop RGEs for all the scalar quartic couplings appearing in (1.2) in the Type-II

2HDM are given by

$$\begin{aligned}
\mathcal{D}\lambda_1 = & \frac{1}{16\pi^2} \left[ \frac{3}{8} (3g_2^4 + g'^4 + 2g_2^2 g'^2) - 3\lambda_1 (3g_2^2 + g'^2) + 24\lambda_1^2 + 2\lambda_3^2 + 2\lambda_3\lambda_4 + \lambda_4^2 \right. \\
& \left. + \lambda_5^2 + 12\lambda_6^2 + 4\lambda_1(3y_b^2 + y_\tau^2) - 6y_b^4 - 2y_\tau^4 \right] \\
& + \frac{1}{256\pi^4} \left[ \frac{1}{16} (291g_2^6 - 101g_2^4 g'^2 - 191g_2^2 g'^4 - 131g'^6) \right. \\
& - \frac{1}{8} (51g_2^4 - 78g_2^2 g'^2 - 217g'^4) \lambda_1 + \frac{5}{2} (3g_2^4 + g'^4) \lambda_3 + \frac{5}{4} (3g_2^4 + 2g_2^2 g'^2 + g'^4) \lambda_4 \\
& + (3g_2^2 + g'^2) (36\lambda_1^2 + 4\lambda_3^2 + 4\lambda_3\lambda_4 + \lambda_4^2 + 18\lambda_6^2) + g'^2 (\lambda_4^2 - \lambda_5^2) - 312\lambda_1^3 \\
& - 8\lambda_3^3 - 6\lambda_4^3 - 20\lambda_1\lambda_3\lambda_4 - 4(5\lambda_1 + 3\lambda_4)\lambda_3^2 - 4(3\lambda_1 + 4\lambda_3)\lambda_4^2 \\
& - 2(7\lambda_1 + 10\lambda_3 + 11\lambda_4)\lambda_5^2 - 2(159\lambda_1 + 33\lambda_3 + 35\lambda_4 + 37\lambda_5)\lambda_6^2 \\
& - 4(9\lambda_3 + 7\lambda_4 + 5\lambda_5)\lambda_6\lambda_7 + 2(3\lambda_1 - 9\lambda_3 - 7\lambda_4 - 5\lambda_5)\lambda_7^2 \\
& - \left\{ \frac{9}{4}g_2^4 - \frac{9}{2}g_2^2 g'^2 - \frac{5}{4}g'^4 - \left( \frac{45}{2}g_2^2 + 80g_3^2 + \frac{25}{6}g'^2 \right) \lambda_1 + 36(4\lambda_1^2 + \lambda_6^2) \right\} y_b^2 \\
& - \left( 32g_3^2 - \frac{4}{3}g'^2 + 3\lambda_1 \right) y_b^4 - 6(2\lambda_3^2 + 2\lambda_3\lambda_4 + \lambda_4^2 + \lambda_5^2 + 6\lambda_6^2) y_\tau^2 \\
& - \left\{ \frac{3}{4}g_2^4 - \frac{11}{2}g_2^2 g'^2 + \frac{25}{4}g'^4 - \frac{5}{2}(3g_2^2 + 5g'^2) \lambda_1 + 12(4\lambda_1^2 + \lambda_6^2) \right\} y_\tau^2 \\
& \left. - (4g'^2 + \lambda_1) y_\tau^4 - 9\lambda_1 y_b^2 y_\tau^2 + 6y_\tau^2 y_b^4 + 30y_b^6 + 10y_\tau^6 \right], \tag{B.10}
\end{aligned}$$

$$\begin{aligned}
\mathcal{D}\lambda_2 = & \frac{1}{16\pi^2} \left[ \frac{3}{8} (3g_2^4 + g'^4 + 2g_2^2 g'^2) - 3\lambda_2 (3g_2^2 + g'^2) + 24\lambda_2^2 + 2\lambda_3^2 + 2\lambda_3\lambda_4 \right. \\
& \left. + \lambda_4^2 + \lambda_5^2 + 12\lambda_7^2 + 12\lambda_2 y_t^2 - 6y_t^4 \right] \\
& + \frac{1}{256\pi^4} \left[ \frac{1}{16} (291g_2^6 - 101g_2^4 g'^2 - 191g_2^2 g'^4 - 131g'^6) \right. \\
& - \frac{1}{8} (51g_2^4 - 78g_2^2 g'^2 - 217g'^4) \lambda_2 + \frac{5}{2} (3g_2^4 + g'^4) \lambda_3 + \frac{5}{4} (3g_2^4 + 2g_2^2 g'^2 + g'^4) \lambda_4 \\
& + (3g_2^2 + g'^2) (36\lambda_2^2 + 4\lambda_3^2 + 4\lambda_3\lambda_4 + \lambda_4^2 + 18\lambda_7^2) + g'^2 (\lambda_4^2 - \lambda_5^2) - 312\lambda_2^3 \\
& - 8\lambda_3^3 - 6\lambda_4^3 - 20\lambda_2\lambda_3\lambda_4 - 4(5\lambda_2 + 3\lambda_4)\lambda_3^2 - 4(3\lambda_2 + 4\lambda_3)\lambda_4^2 \\
& - 2(7\lambda_2 + 10\lambda_3 + 11\lambda_4)\lambda_5^2 + 2(3\lambda_2 - 9\lambda_3 - 7\lambda_4 - 5\lambda_5)\lambda_6^2 \\
& - 4(9\lambda_3 + 7\lambda_4 + 5\lambda_5)\lambda_6\lambda_7 - 2(159\lambda_2 + 33\lambda_3 + 35\lambda_4 + 37\lambda_5)\lambda_7^2 \\
& - 6(2\lambda_3^2 + 2\lambda_3\lambda_4 + \lambda_4^2 + \lambda_5^2 + 6\lambda_7^2) y_b^2 - \left\{ \frac{9}{4}g_2^4 - \frac{21}{2}g_2^2 g'^2 + \frac{19}{4}g'^4 \right. \\
& \left. - \left( \frac{45}{2}g_2^2 + 80g_3^2 + \frac{85}{6}g'^2 \right) \lambda_2 + 36(4\lambda_2^2 + \lambda_7^2) \right\} y_t^2 - 9\lambda_2 y_b^2 y_t^2 + 6y_b^2 y_t^4 \\
& \left. - \left( 32g_3^2 + \frac{8}{3}g'^2 + 3\lambda_2 \right) y_t^4 + 30y_t^6 - 2(2\lambda_3^2 + 2\lambda_3\lambda_4 + \lambda_4^2 + \lambda_5^2 + 6\lambda_7^2) y_\tau^2 \right], \tag{B.11}
\end{aligned}$$

$$\begin{aligned}
\mathcal{D}\lambda_3 = & \frac{1}{16\pi^2} \left[ \frac{3}{4}(3g_2^4 + g'^4 - 2g_2^2g'^2) - 3\lambda_3(3g_2^2 + g'^2) + 4(\lambda_1 + \lambda_2)(3\lambda_3 + \lambda_4) + 4\lambda_3^2 \right. \\
& \left. + 2(\lambda_4^2 + \lambda_5^2) + 4(\lambda_6^2 + \lambda_7^2 + 4\lambda_6\lambda_7) + 2\lambda_3(3y_b^2 + y_\tau^2 + 3y_t^2) - 12y_b^2y_t^2 \right] \\
& + \frac{1}{256\pi^4} \left[ \frac{1}{8} (291g_2^6 + 11g_2^4g'^2 + 101g_2^2g'^4 - 131g'^6) \right. \\
& + \frac{5}{2} (9g_2^4 - 2g_2^2g'^2 + 3g'^4) (\lambda_1 + \lambda_2) - \frac{1}{8} (111g_2^4 - 22g_2^2g'^2 - 197g'^4)\lambda_3 \\
& + 2(3g_2^2 + g'^2)[12(\lambda_1 + \lambda_2)\lambda_3 + \lambda_3^2 + \lambda_4^2] - 4(\lambda_1^2 + \lambda_2^2)(15\lambda_3 + 4\lambda_4) \\
& - 4(\lambda_1 + \lambda_2)(18\lambda_3^2 + 7\lambda_4^2 + 8\lambda_3\lambda_4 + 9\lambda_5^2) - 12(\lambda_3^3 + \lambda_4^3 + g_2^2\lambda_3\lambda_4) \\
& + \left( \frac{15}{2}g_2^4 - 3g_2^2g'^2 + \frac{5}{2}g'^4 \right) \lambda_4 + 4(9g_2^2 + 2g'^2)(\lambda_1 + \lambda_2)\lambda_4 \\
& - 4\lambda_3\lambda_4(\lambda_3 + 4\lambda_4) - 2(9\lambda_3 + 22\lambda_4)\lambda_5^2 - 4g'^2(\lambda_4^2 - \lambda_5^2) + 2g'^2(\lambda_6^2 + \lambda_7^2) \\
& - 4(31\lambda_1 + 11\lambda_2)\lambda_6^2 - 4(15\lambda_3 + 17\lambda_4 + 17\lambda_5)(\lambda_6^2 + \lambda_7^2) + 4(27g_2^2 + 8g'^2)\lambda_6\lambda_7 \\
& - 8[11(\lambda_1 + \lambda_2 + 2\lambda_3 + \lambda_4) + 9\lambda_5]\lambda_6\lambda_7 - 4(11\lambda_1 + 31\lambda_2)\lambda_7^2 \\
& - \left\{ \frac{1}{4}(9g_2^4 - 5g'^4 + 18g_2^2g'^2) - (40g_3^2 + \frac{45}{4}g_2^2 + \frac{25}{12}g'^2)\lambda_3 \right\} y_b^2 \\
& - \frac{1}{4} \left\{ 3g_2^4 + 25g'^4 + 22g_2^2g'^2 - 5(3g_2^2 + 5g'^2)\lambda_3 \right\} y_\tau^2 \\
& - 2 \left\{ 2\lambda_3^2 + \lambda_4^2 + 4\lambda_1(3\lambda_3 + \lambda_4) + \lambda_5^2 + 4\lambda_6^2 + 8\lambda_6\lambda_7 \right\} (3y_b^2 + y_\tau^2) \\
& - \left\{ \frac{9}{4}g_2^4 + \frac{21}{2}g_2^2g'^2 + \frac{19}{4}g'^4 - \left( 40g_3^2 + \frac{45}{4}g_2^2 + \frac{85}{12}g'^2 \right) \lambda_3 \right. \\
& \left. + 6(12\lambda_2\lambda_3 + 2\lambda_3^2 + 4\lambda_2\lambda_4 + \lambda_4^2 + \lambda_5^2 + 8\lambda_6\lambda_7 + 4\lambda_7^2) \right\} y_t^2 \\
& \left. - (64g_3^2 + \frac{4}{3}g'^2 - 15\lambda_3)y_b^2y_t^2 + 36y_b^4y_t^2 - \frac{9}{2}\lambda_3[3(y_b^4 + y_t^4) + y_\tau^4] + 36y_b^2y_t^4 \right], \quad (\text{B.12})
\end{aligned}$$

$$\begin{aligned}
\mathcal{D}\lambda_4 = & \frac{1}{16\pi^2} \left[ 3g_2^2g'^2 - 3\lambda_4(3g_2^2 + g'^2) + 4(\lambda_1 + \lambda_2 + 2\lambda_3)\lambda_4 + 4\lambda_4^2 + 8\lambda_5^2 \right. \\
& \left. + 10(\lambda_6^2 + \lambda_7^2) + 4\lambda_6\lambda_7 + 2\lambda_4\{3(y_b^2 + y_t^2) + y_\tau^2\} + 12y_b^2y_t^2 \right] \\
& + \frac{1}{256\pi^4} \left[ -14g_2^4g'^2 - \frac{73}{2}g_2^2g'^4 + 2g_2^2g'^2\{5(\lambda_1 + \lambda_2) + \lambda_3\} \right. \\
& - \frac{1}{8}(231g_2^4 - 102g_2^2g'^2 - 157g'^4)\lambda_4 + 4\{2g'^2(\lambda_1 + \lambda_2) - 7(\lambda_1^2 + \lambda_2^2 + \lambda_3^2)\}\lambda_4 \\
& + 4(9g_2^2 + g'^2)\lambda_3\lambda_4 - 40(\lambda_1 + \lambda_2)(2\lambda_3\lambda_4 + \lambda_4^2) + 2(9g_2^2 + 4g'^2)\lambda_4^2 - 28\lambda_3\lambda_4^2 \\
& + 2(27g_2^2 + 8g'^2)\lambda_5^2 - 48(\lambda_1 + \lambda_2 + \lambda_3)\lambda_5^2 - 26\lambda_4\lambda_5^2 + 8g'^2\lambda_6\lambda_7 \\
& + 2\{27g_2^2 + 7g'^2 - 2(18\lambda_3 + 17\lambda_4 + 20\lambda_5)\}\lambda_6^2 + \lambda_7^2 - 4(37\lambda_1 + 5\lambda_2)\lambda_6^2 \\
& - 8\{5(\lambda_1 + \lambda_2 + 2\lambda_3 + 4\lambda_4) + 12\lambda_5\}\lambda_6\lambda_7 - 4(5\lambda_1 + 37\lambda_2)\lambda_7^2 \\
& \left. + \left\{ 9g_2^2g'^2 + (40g_3^2 + \frac{45}{4}g_2^2 + \frac{25}{12}g'^2)\lambda_4 - 12[2(\lambda_1 + \lambda_3)\lambda_4 + \lambda_4^2 + 2\lambda_5^2] \right\} \right]
\end{aligned}$$

$$\begin{aligned}
& + 5\lambda_6^2 + \lambda_6\lambda_7 \} y_b^2 + \left\{ 21g_2^2g'^2 + (40g_3^2 + \frac{45}{4}g_2^2 + \frac{85}{12}g'^2)\lambda_4 - 12[2(\lambda_2 + \lambda_3)\lambda_4 \right. \\
& + \lambda_4^2 + 2\lambda_5^2 + \lambda_6\lambda_7 + 5\lambda_7^2] \} y_t^2 + \left( 64g_3^2 + \frac{4}{3}g'^2 - 24\lambda_3 - 33\lambda_4 \right) y_b^2 y_t^2 \\
& + \left\{ 11g_2^2g'^2 + \frac{5}{4}(3g_2^2 + 5g'^2)\lambda_4 - 4[2(\lambda_1 + \lambda_3)\lambda_4 + \lambda_4^2 + 2\lambda_5^2 \right. \\
& \left. + 5\lambda_6^2 + \lambda_6\lambda_7] \} y_\tau^2 - \frac{9}{2}\lambda_4 \{ 3(y_b^4 + y_t^4) + y_\tau^4 \} - 24y_b^2 y_t^2 (y_b^2 + y_t^2) \right] , \tag{B.13}
\end{aligned}$$

$$\begin{aligned}
\mathcal{D}\lambda_5 = & \frac{1}{16\pi^2} \left[ -3\lambda_5(3g_2^2 + g'^2) + 4(\lambda_1 + \lambda_2 + 2\lambda_3 + 3\lambda_4)\lambda_5 + 10(\lambda_6^2 + \lambda_7^2) \right. \\
& \left. + 4\lambda_6\lambda_7 + 2\lambda_5 \{ 3(y_b^2 + y_t^2) + y_\tau^2 \} \right] \\
& + \frac{1}{256\pi^4} \left[ -\frac{1}{8} (231g_2^4 - 38g_2^2g'^2 - 157g'^4) \lambda_5 + 4(9g_2^2 + 4g'^2)\lambda_3\lambda_5 \right. \\
& - 4 \{ g'^2(\lambda_1 + \lambda_2) + 7(\lambda_1^2 + \lambda_2^2 + \lambda_3^2) \} \lambda_5 - 8(\lambda_1 + \lambda_2)(10\lambda_3 + 11\lambda_4)\lambda_5 \\
& + 4 \{ 6(3g_2^2 + g'^2) - 19\lambda_3 - 8\lambda_4 \} \lambda_4\lambda_5 + 6\lambda_5^3 - 4(37\lambda_1 + 5\lambda_2)\lambda_6^2 \\
& - 4(5\lambda_1 + 37\lambda_2)\lambda_7^2 + 2 \{ 27g_2^2 + 10g'^2 - 2(18\lambda_3 + 19\lambda_4 + 18\lambda_5) \} (\lambda_6^2 + \lambda_7^2) \\
& - 4 \{ g'^2 + 10(\lambda_1 + \lambda_2 + 2\lambda_3) + 22\lambda_4 + 42\lambda_5 \} \lambda_6\lambda_7 \\
& + \left\{ (40g_3^2 + \frac{45}{4}g_2^2 + \frac{25}{12}g'^2)\lambda_5 - 12[2(\lambda_1 + \lambda_3)\lambda_5 + 3\lambda_4\lambda_5 + 5\lambda_6^2 + \lambda_6\lambda_7] \right\} y_b^2 \\
& + \left\{ (40g_3^2 + \frac{45}{4}g_2^2 + \frac{85}{12}g'^2)\lambda_5 - 12[2(\lambda_2 + \lambda_3)\lambda_5 + 3\lambda_4\lambda_5 + \lambda_6\lambda_7 + 5\lambda_7^2] \right\} y_t^2 \\
& + \left\{ (\frac{15}{4}g_2^2 + \frac{25}{4}g'^2)\lambda_5 - 8(\lambda_1 + \lambda_3)\lambda_5 - 12\lambda_4\lambda_5 - 20\lambda_6^2 - 4\lambda_6\lambda_7 \right\} y_\tau^2 \\
& \left. - \frac{1}{2}\lambda_5 \{ 3(y_b^4 + y_t^4) + y_\tau^4 \} - 33\lambda_5 y_b^2 y_t^2 \right] , \tag{B.14}
\end{aligned}$$

$$\begin{aligned}
\mathcal{D}\lambda_6 = & \frac{1}{16\pi^2} \left[ -3\lambda_6(3g_2^2 + g'^2) + 2(12\lambda_1 + 3\lambda_3 + 4\lambda_4)\lambda_6 + 2(3\lambda_3 + 2\lambda_4)\lambda_7 \right. \\
& \left. + 10\lambda_5\lambda_6 + 2\lambda_5\lambda_7 + 3\lambda_6(3y_b^2 + y_t^2 + y_\tau^2) \right] \\
& + \frac{1}{256\pi^4} \left[ -\frac{1}{8} (141g_2^4 - 58g_2^2g'^2 - 187g'^4) \lambda_6 + 6(3g_2^2 + g'^2)(6\lambda_1 + \lambda_3)\lambda_6 \right. \\
& - 6(53\lambda_1^2 - \lambda_2^2)\lambda_6 - 4(33\lambda_1 + 9\lambda_2 + 8\lambda_3)\lambda_3\lambda_6 + 2(18g_2^2 + 5g'^2)\lambda_4\lambda_6 \\
& - 2(70\lambda_1 + 14\lambda_2 + 34\lambda_3 + 17\lambda_4)\lambda_4\lambda_6 + 2(27g_2^2 + 10g'^2)\lambda_5\lambda_6 \\
& - 4(37\lambda_1 + 5\lambda_2 + 18\lambda_3 + 19\lambda_4 + 9\lambda_5)\lambda_5\lambda_6 - 111\lambda_6^3 - 42\lambda_7^3 \\
& + \frac{5}{4}(9g_2^4 + 2g_2^2g'^2 + 3g'^4)\lambda_7 + 12(3g_2^2 + g'^2)\lambda_3\lambda_7 - 36(\lambda_1 + \lambda_2 + \lambda_3)\lambda_3\lambda_7 \\
& + 2(9g_2^2 + 4g'^2)\lambda_4\lambda_7 - 2 \{ 14(\lambda_1 + \lambda_2 + 2\lambda_3) + 17\lambda_4 \} \lambda_4\lambda_7 \\
& - 2 \{ g'^2 + 10(\lambda_1 + \lambda_2 + 2\lambda_3) + 22\lambda_4 + 21\lambda_5 \} \lambda_5\lambda_7 - 3(42\lambda_6 + 11\lambda_7)\lambda_6\lambda_7 \\
& \left. + \left\{ 60g_3^2 + \frac{135}{8}g_2^2 + \frac{25}{8}g'^2 - 6(24\lambda_1 + 3\lambda_3 + 4\lambda_4 + 5\lambda_5) \right\} \lambda_6 y_b^2 \right]
\end{aligned}$$

$$\begin{aligned}
& + \left\{ 20g_3^2 + \frac{45}{8}g_2^2 + \frac{85}{24}g'^2 - 6(3\lambda_3 + 4\lambda_4 + 5\lambda_5) \right\} \lambda_6 y_t^2 \\
& + \left\{ \frac{15}{8}(3g_2^2 + 5g'^2) - 2(24\lambda_1 + 3\lambda_3 + 4\lambda_4 + 5\lambda_5) \right\} \lambda_6 y_\tau^2 \\
& - 12(3\lambda_3 + 2\lambda_4 + \lambda_5)\lambda_7 y_t^2 - \frac{1}{4}(27y_t^4 + 33y_b^4 + 11y_\tau^4)\lambda_6 - 21\lambda_6 y_b^2 y_t^2 \Big], \quad (\text{B.15})
\end{aligned}$$

$$\begin{aligned}
\mathcal{D}\lambda_7 = & \frac{1}{16\pi^2} \left[ -3\lambda_7(3g_2^2 + g'^2) + 2(12\lambda_2 + 3\lambda_3 + 4\lambda_4)\lambda_7 + 2(3\lambda_3 + 2\lambda_4)\lambda_6 \right. \\
& \left. + 10\lambda_5\lambda_7 + 2\lambda_5\lambda_6 + \lambda_7(3y_b^2 + 9y_t^2 + y_\tau^2) \right] \\
& + \frac{1}{256\pi^4} \left[ \frac{5}{4}(9g_2^4 + 2g_2^2 g'^2 + 3g'^4)\lambda_6 + 12(3g_2^2 + g'^2)\lambda_3\lambda_6 \right. \\
& - 36(\lambda_1 + \lambda_2 + \lambda_3)\lambda_3\lambda_6 + 2(9g_2^2 + 4g'^2)\lambda_4\lambda_6 - 28(\lambda_1 + \lambda_2 + 2\lambda_3)\lambda_4\lambda_6 \\
& - 34\lambda_4^2\lambda_6 - 2g'^2\lambda_5\lambda_6 - 4\{5(\lambda_1 + \lambda_2 + 2\lambda_3) + 11\lambda_4\}\lambda_5\lambda_6 - 42(\lambda_5^2 + \lambda_6^2)\lambda_6 \\
& - \frac{1}{8}(141g_2^4 - 58g_2^2 g'^2 - 187g'^4)\lambda_7 + 6\lambda_1^2\lambda_7 + 36(3g_2^2 + g'^2)\lambda_2\lambda_7 - 318\lambda_2^2\lambda_7 \\
& + 6(3g_2^2 + g'^2)\lambda_3\lambda_7 - 12(3\lambda_1 + 11\lambda_2)\lambda_3\lambda_7 - 32\lambda_3^2\lambda_7 + 2(18g_2^2 + 5g'^2)\lambda_4\lambda_7 \\
& - 4(7\lambda_1 + 35\lambda_2 + 17\lambda_3)\lambda_4\lambda_7 - 34\lambda_4^2\lambda_7 + 2(27g_2^2 + 10g'^2)\lambda_5\lambda_7 \\
& - 4(5\lambda_1 + 37\lambda_2 + 18\lambda_3 + 19\lambda_4)\lambda_5\lambda_7 - 36\lambda_5^2\lambda_7 - 33\lambda_6^2\lambda_7 \\
& - 126\lambda_6\lambda_7^2 - 111\lambda_7^3 - 12(3\lambda_3 + 2\lambda_4 + \lambda_5)\lambda_6 y_b^2 \\
& + \left\{ 20g_3^2 + \frac{45}{8}g_2^2 + \frac{25}{24}g'^2 - 6(3\lambda_3 + 4\lambda_4 + 5\lambda_5) \right\} \lambda_7 y_b^2 \\
& + \left\{ 60g_3^2 + \frac{135}{8}g_2^2 + \frac{85}{8}g'^2 - 6(24\lambda_2 + 3\lambda_3 + 4\lambda_4 + 5\lambda_5) \right\} \lambda_7 y_t^2 \\
& - 4(3\lambda_3 + 2\lambda_4 + \lambda_5)\lambda_6 y_\tau^2 + \left\{ \frac{5}{8}(3g_2^2 + 5g'^2) - 2(3\lambda_3 + 4\lambda_4 + 5\lambda_5) \right\} \lambda_7 y_\tau^2 \\
& \left. - \frac{1}{4}(33y_t^4 + 27y_b^4 + 9y_\tau^4)\lambda_7 - 21\lambda_7 y_b^2 y_t^2 \right]. \quad (\text{B.16})
\end{aligned}$$

The two-loop RGE for the soft mass parameter is given by

$$\begin{aligned}
\mathcal{D}(m_{12}^2) = & \frac{1}{16\pi^2} \left[ -\frac{3}{2}(3g_2^2 + g'^2)m_{12}^2 + 2(\lambda_3 + 2\lambda_4 + 3\lambda_5)m_{12}^2 \right. \\
& \left. + 2(3y_b^2 + 3y_t^2 + y_\tau^2)m_{12}^2 + 12(\lambda_6\mu_1^2 + \lambda_7\mu_2^2) \right] \\
& + \frac{1}{256\pi^4} \left[ -\frac{1}{16}(243g_2^4 - 30g_2^2 g'^2 - 153g'^4)m_{12}^2 + 3\{2\lambda_1^2 + \lambda_2^2\} + \lambda_5^2 \right. \\
& + 4(\lambda_6^2 + \lambda_7^2)\}m_{12}^2 + 4(3g_2^2 + g'^2)(\lambda_3 + 2\lambda_4 + 3\lambda_5)m_{12}^2 \\
& - 12(\lambda_1 + \lambda_2)\lambda_{345}m_{12}^2 - 6(\lambda_3\lambda_4 + 2\lambda_3\lambda_5 + 2\lambda_4\lambda_5 + 6\lambda_6\lambda_7)m_{12}^2 \\
& \left. + \left\{ 20g_3^2 + \frac{45}{8}g_2^2 + \frac{25}{24}g'^2 - 6(\lambda_3 + 2\lambda_4 + 3\lambda_5) \right\} y_b^2 m_{12}^2 \right]
\end{aligned}$$

$$\begin{aligned}
& + \left\{ 20g_3^2 + \frac{45}{8}g_2^2 + \frac{85}{24}g'^2 - 6(\lambda_3 + 2\lambda_4 + 3\lambda_5) \right\} y_t^2 m_{12}^2 \\
& + \left\{ \frac{5}{8}(3g_2^2 + 5g'^2) - 2(\lambda_3 + 2\lambda_4 + 3\lambda_5) \right\} y_\tau^2 m_{12}^2 \\
& + 24(3g_2^2 + g'^2)(\lambda_6\mu_1^2 + \lambda_7\mu_2^2) - 72(\lambda_1\lambda_6\mu_1^2 + \lambda_2\lambda_7\mu_2^2) \\
& - 12\lambda_{345}\{(2\lambda_6 + \lambda_7)\mu_1^2 + (\lambda_6 + 2\lambda_7)\mu_2^2\} \\
& - 24\{(3y_b^2 + y_\tau^2)\lambda_6\mu_1^2 + 3y_t^2\lambda_7\mu_2^2\} - \frac{9}{4}(3y_b^4 + 3y_t^4 + y_\tau^4)m_{12}^2 \Big] \quad (\text{B.17})
\end{aligned}$$

Finally, the two-loop RGE for the soft mass parameter is given by

$$\begin{aligned}
\mathcal{D}(m_{12}^2) = & \frac{1}{16\pi^2} \left[ -\frac{3}{2}(3g_2^2 + g'^2)m_{12}^2 + 2(\lambda_3 + 2\lambda_4 + 3\lambda_5)m_{12}^2 \right. \\
& \left. + 2(3y_b^2 + 3y_t^2 + y_\tau^2)m_{12}^2 + 12(\lambda_6\mu_1^2 + \lambda_7\mu_2^2) \right] \\
& + \frac{1}{256\pi^4} \left[ -\frac{1}{16}(243g_2^4 - 30g_2^2g'^2 - 153g'^4)m_{12}^2 + 3\{2\lambda_1^2 + \lambda_2^2\} + \lambda_5^2 \right. \\
& + 4(\lambda_6^2 + \lambda_7^2)\}m_{12}^2 + 4(3g_2^2 + g'^2)(\lambda_3 + 2\lambda_4 + 3\lambda_5)m_{12}^2 \\
& - 12(\lambda_1 + \lambda_2)\lambda_{345}m_{12}^2 - 6(\lambda_3\lambda_4 + 2\lambda_3\lambda_5 + 2\lambda_4\lambda_5 + 6\lambda_6\lambda_7)m_{12}^2 \\
& + \left\{ 20g_3^2 + \frac{45}{8}g_2^2 + \frac{25}{24}g'^2 - 6(\lambda_3 + 2\lambda_4 + 3\lambda_5) \right\} y_b^2 m_{12}^2 \\
& + \left\{ 20g_3^2 + \frac{45}{8}g_2^2 + \frac{85}{24}g'^2 - 6(\lambda_3 + 2\lambda_4 + 3\lambda_5) \right\} y_t^2 m_{12}^2 \\
& + \left\{ \frac{5}{8}(3g_2^2 + 5g'^2) - 2(\lambda_3 + 2\lambda_4 + 3\lambda_5) \right\} y_\tau^2 m_{12}^2 \\
& + 24(3g_2^2 + g'^2)(\lambda_6\mu_1^2 + \lambda_7\mu_2^2) - 72(\lambda_1\lambda_6\mu_1^2 + \lambda_2\lambda_7\mu_2^2) \\
& - 12\lambda_{345}\{(2\lambda_6 + \lambda_7)\mu_1^2 + (\lambda_6 + 2\lambda_7)\mu_2^2\} \\
& \left. - 24\{(3y_b^2 + y_\tau^2)\lambda_6\mu_1^2 + 3y_t^2\lambda_7\mu_2^2\} - \frac{9}{4}(3y_b^4 + 3y_t^4 + y_\tau^4)m_{12}^2 \right] \quad (\text{B.18})
\end{aligned}$$

Note that the mass parameters  $\mu_{1,2}^2$  are removed by the tadpole conditions:

$$\frac{\partial V}{\partial v_1} = 0 = -\mu_1^2 v_1 - m_{12}^2 v_2 + \frac{1}{2} [2\lambda_1 v_1^3 + \lambda_{345} v_1 v_2^2 + 3\lambda_6 v_1^2 v_2 + \lambda_7 v_2^3], \quad (\text{B.19})$$

$$\frac{\partial V}{\partial v_2} = 0 = -\mu_2^2 v_2 - m_{12}^2 v_1 + \frac{1}{2} [2\lambda_2 v_2^3 + \lambda_{345} v_2 v_1^2 + \lambda_6 v_1^3 + 3\lambda_7 v_2 v_1^2], \quad (\text{B.20})$$

and hence, it is not necessary to write down their RGEs explicitly.

## References

- [1] G. Aad *et al.* [ATLAS Collaboration], Phys. Lett. B **716**, 1 (2012) [arXiv:1207.7214 [hep-ex]].
- [2] S. Chatrchyan *et al.* [CMS Collaboration], Phys. Lett. B **716**, 30 (2012) [arXiv:1207.7235 [hep-ex]].

- [3] ATLAS collaboration, ATLAS-CONF-2014-009.
- [4] CMS Collaboration, CMS-PAS-HIG-14-009.
- [5] J. F. Gunion, H. E. Haber, G. Kane and S. Dawson, *The Higgs Hunter's Guide*, Addison-Wesley (1990).
- [6] For a review, see e.g. G. C. Branco, P. M. Ferreira, L. Lavoura, M. N. Rebelo, M. Sher and J. P. Silva, Phys. Rept. **516**, 1 (2012) [arXiv:1106.0034 [hep-ph]].
- [7] R. A. Battye, G. D. Brawn and A. Pilaftsis, JHEP **1108**, 020 (2011) [arXiv:1106.3482 [hep-ph]].
- [8] S. L. Glashow and S. Weinberg, Phys. Rev. D **15**, 1958 (1977).
- [9] E. A. Paschos, Phys. Rev. D **15**, 1966 (1977).
- [10] A. Pich and P. Tuzon, Phys. Rev. D **80**, 091702 (2009) [arXiv:0908.1554 [hep-ph]].
- [11] ATLAS collaboration, ATLAS-CONF-2014-010.
- [12] A. Celis, V. Ilisie and A. Pich, JHEP **1307**, 053 (2013) [arXiv:1302.4022 [hep-ph]].
- [13] C.-Y. Chen, S. Dawson and M. Sher, Phys. Rev. D **88**, 015018 (2013) [arXiv:1305.1624 [hep-ph]].
- [14] N. Craig, J. Galloway and S. Thomas, arXiv:1305.2424 [hep-ph].
- [15] K. Cheung, J. S. Lee and P.-Y. Tseng, JHEP **1401**, 085 (2014) [arXiv:1310.3937 [hep-ph]].
- [16] L. Wang and X. -F. Han, arXiv:1404.7437 [hep-ph].
- [17] B. Dumont, J. F. Gunion, Y. Jiang and S. Kraml, arXiv:1405.3584 [hep-ph].
- [18] S. Kanemura, K. Tsumura, K. Yagyu and H. Yokoya, arXiv:1406.3294 [hep-ph].
- [19] C. W. Chiang and K. Yagyu, JHEP **1307**, 160 (2013) [arXiv:1303.0168 [hep-ph]].
- [20] B. Grinstein and P. Uttayarat, JHEP **1306**, 094 (2013) [Erratum-ibid. **1309**, 110 (2013)] [arXiv:1304.0028 [hep-ph]].
- [21] O. Eberhardt, U. Nierste and M. Wiebusch, JHEP **1307**, 118 (2013) [arXiv:1305.1649 [hep-ph]].
- [22] J. Baglio, O. Eberhardt, U. Nierste and M. Wiebusch, Phys. Rev. D **90**, 015008 (2014) [arXiv:1403.1264 [hep-ph]].
- [23] P. H. Chankowski, T. Farris, B. Grzadkowski, J. F. Gunion, J. Kalinowski and M. Krawczyk, Phys. Lett. B **496**, 195 (2000) [hep-ph/0009271].
- [24] J. F. Gunion and H. E. Haber, Phys. Rev. D **67**, 075019 (2003) [hep-ph/0207010].
- [25] I. F. Ginzburg and M. Krawczyk, Phys. Rev. D **72**, 115013 (2005) [hep-ph/0408011].
- [26] M. Carena, I. Low, N. R. Shah and C. E. M. Wagner, JHEP **1404**, 015 (2014) [arXiv:1310.2248 [hep-ph]].
- [27] A. Delgado, G. Nardini and M. Quiros, JHEP **1307**, 054 (2013) [arXiv:1303.0800 [hep-ph]].
- [28] C. C. Nishi, Phys. Rev. D **83**, 095005 (2011) [arXiv:1103.0252 [hep-ph]].
- [29] A. Pilaftsis, Phys. Lett. B **706**, 465 (2012) [arXiv:1109.3787 [hep-ph]].
- [30] M. Maniatis, A. von Manteuffel and O. Nachtmann, Eur. Phys. J. C **57** (2008) 719 [arXiv:0707.3344 [hep-ph]].

- [31] I. P. Ivanov, Phys. Rev. D **77** (2008) 015017 [arXiv:0710.3490 [hep-ph]].
- [32] C. C. Nishi, Phys. Rev. D **77** (2008) 055009 [arXiv:0712.4260 [hep-ph]].
- [33] N. G. Deshpande and E. Ma, Phys. Rev. D **18**, 2574 (1978).
- [34] J. Patera, R. T. Sharp and R. Slansky, J. Math. Phys. **21**, 2335 (1980).
- [35] R. Slansky, Phys. Rept. **79**, 1 (1981).
- [36] P. Sikivie, L. Susskind, M. B. Voloshin and V. I. Zakharov, Nucl. Phys. B **173** (1980) 189.
- [37] J. F. Gunion and H. E. Haber, Phys. Rev. D **72**, 095002 (2005) [hep-ph/0506227].
- [38] M. Maniatis and O. Nachtmann, JHEP **1111**, 151 (2011) [arXiv:1106.1436 [hep-ph]].
- [39] J. Goldstone, Nuovo Cim. **19**, 154 (1961).
- [40] K. A. Olive *et al.* (Particle Data Group), Chin. Phys. C **38**, 090001 (2014) [<http://pdg.lbl.gov/>].
- [41] R. D. Peccei and H. R. Quinn, Phys. Rev. Lett. **38**, 1440 (1977).
- [42] H. E. Haber and R. Hempfling, Phys. Rev. D **48**, 4280 (1993) [hep-ph/9307201].
- [43] A. Pilaftsis and C. E. M. Wagner, Nucl. Phys. B **553**, 3 (1999) [hep-ph/9902371].
- [44] H. Georgi and D. V. Nanopoulos, Phys. Lett. B **82**, 95 (1979).
- [45] J. F. Donoghue and L. F. Li, Phys. Rev. D **19**, 945 (1979).
- [46] L. Lavoura and J. P. Silva, Phys. Rev. D **50**, 4619 (1994) [hep-ph/9404276].
- [47] F. J. Botella and J. P. Silva, Phys. Rev. D **51**, 3870 (1995) [hep-ph/9411288].
- [48] M. Carena, H. E. Haber, I. Low, N. R. Shah and C. E. M. Wagner, arXiv:1410.4969 [hep-ph].
- [49] R. Barbieri, L. J. Hall and V. S. Rychkov, Phys. Rev. D **74**, 015007 (2006) [hep-ph/0603188].
- [50] G. Aad *et al.* [ATLAS Collaboration], arXiv:1406.3827 [hep-ex].
- [51] M. Ciuchini, G. Degrossi, P. Gambino and G. F. Giudice, Nucl. Phys. B **527**, 21 (1998) [hep-ph/9710335].
- [52] F. Borzumati and C. Greub, Phys. Rev. D **58**, 074004 (1998) [hep-ph/9802391]; *ibid.* **59**, 057501 (1999) [hep-ph/9809438].
- [53] T. Hermann, M. Misiak and M. Steinhauser, JHEP **1211**, 036 (2012) [arXiv:1208.2788 [hep-ph]].
- [54] O. Deschamps, S. Descotes-Genon, S. Monteil, V. Niess, S. T'Jampens and V. Tisserand, Phys. Rev. D **82**, 073012 (2010) [arXiv:0907.5135 [hep-ph]].
- [55] D. Eriksson, J. Rathsman and O. Stal, Comput. Phys. Commun. **181**, 189 (2010) [arXiv:0902.0851 [hep-ph]]; <http://2hdmc.hepforge.org/>
- [56] CMS Collaboration, CMS-PAS-HIG-14-020.
- [57] ATLAS collaboration, ATLAS-CONF-2014-050.
- [58] ATLAS collaboration, ATLAS-CONF-2013-090.
- [59] CMS Collaboration, CMS-PAS-HIG-13-035.
- [60] G. Aad *et al.* [ATLAS Collaboration], Eur. Phys. J. C **73**, 2465 (2013) [arXiv:1302.3694 [hep-ex]].

- [61] S. Heinemeyer *et al.* [LHC Higgs Cross Section Working Group Collaboration], arXiv:1307.1347 [hep-ph].
- [62] B. Coleppa, F. Kling and S. Su, arXiv:1408.4119 [hep-ph].
- [63] CMS Collaboration, CMS-PAS-HIG-13-026.
- [64] J. Alwall *et al.*, JHEP **1407**, 079 (2014) [arXiv:1405.0301 [hep-ph]]; <https://launchpad.net/mg5amcnlo>.
- [65] R. D. Ball *et al.*, Nucl. Phys. B **867**, 244 (2013) [arXiv:1207.1303 [hep-ph]]; <https://nnpdf.hepforge.org/>
- [66] M. Flechl, R. Klees, M. Kramer, M. Spira and M. Ubiali, arXiv:1409.5615 [hep-ph].
- [67] M. Cacciari, G. P. Salam and G. Soyez, JHEP **0804**, 063 (2008) [arXiv:0802.1189 [hep-ph]].
- [68] G. Bevilacqua, M. Czakon, C. G. Papadopoulos, R. Pittau and M. Worek, JHEP **0909**, 109 (2009) [arXiv:0907.4723 [hep-ph]].
- [69] C. G. Lester and D. J. Summers, Phys. Lett. B **463**, 99 (1999) [hep-ph/9906349].
- [70] CMS Collaboration, CMS-PAS-TOP-14-015.
- [71] S. Chatrchyan *et al.* [CMS Collaboration], JHEP **1401**, 096 (2014) [arXiv:1312.1129 [hep-ex]].
- [72] CMS Collaboration, CMS-PAS-HIG-13-027.
- [73] S. Chatrchyan *et al.* [CMS Collaboration], Phys. Rev. D **89**, 092007 (2014) [arXiv:1312.5353 [hep-ex]].
- [74] V. Khachatryan *et al.* [CMS Collaboration], arXiv:1408.3316 [hep-ex].
- [75] ATLAS Collaboration, ATLAS-CONF-2014-049.
- [76] CMS Collaboration, CMS-PAS-HIG-14-006.
- [77] G. Aad *et al.* [ATLAS Collaboration], Phys. Rev. Lett. **113**, no. 17, 171801 (2014) [arXiv:1407.6583 [hep-ex]].
- [78] V. Barger, L. L. Everett, C. B. Jackson, A. Peterson and G. Shaughnessy, arXiv:1408.0003 [hep-ph].
- [79] G. Aad *et al.* [ATLAS Collaboration], arXiv:1406.5053 [hep-ex].
- [80] V. Khachatryan *et al.* [CMS Collaboration], arXiv:1410.2751 [hep-ex].
- [81] M. Spira and J. D. Wells, Nucl. Phys. B **523**, 3 (1998) [hep-ph/9711410].
- [82] A. Pomarol and J. Serra, Phys. Rev. D **78**, 074026 (2008) [arXiv:0806.3247 [hep-ph]].
- [83] K. Kumar, T. M. P. Tait and R. Vega-Morales, JHEP **0905**, 022 (2009) [arXiv:0901.3808 [hep-ph]].
- [84] S. Jung and J. D. Wells, JHEP **1011**, 001 (2010) [arXiv:1008.0870 [hep-ph]].
- [85] G. Cacciapaglia, R. Chierici, A. Deandrea, L. Panizzi, S. Perries and S. Tosi, JHEP **1110**, 042 (2011) [arXiv:1107.4616 [hep-ph]].
- [86] G. L. Kane, E. Kuflik, R. Lu and L. T. Wang, Phys. Rev. D **84**, 095004 (2011) [arXiv:1101.1963 [hep-ph]].
- [87] ATLAS Collaboration, ATLAS-CONF-2013-051.
- [88] V. Khachatryan *et al.* [CMS Collaboration], arXiv:1409.7339 [hep-ex].

- [89] G. Bevilacqua and M. Worek, JHEP **1207**, 111 (2012) [arXiv:1206.3064 [hep-ph]].
- [90] D. Paredes [ATLAS Collaboration], PhD Thesis, Université Blaise Pascal (2013), CERN-THESIS-2013-202.
- [91] G. Bevilacqua, M. Czakon, M. Krmer, M. Kubocz and M. Worek, JHEP **1307**, 095 (2013) [arXiv:1304.6860 [hep-ph]].
- [92] R. V. Harlander, S. Liebler and H. Mantler, Comput. Phys. Commun. **184**, 1605 (2013) [arXiv:1212.3249 [hep-ph]]; <http://sushi.hepforge.org/>
- [93] M. H. Seymour, Z. Phys. C **62**, 127 (1994).
- [94] J. M. Butterworth, A. R. Davison, M. Rubin and G. P. Salam, Phys. Rev. Lett. **100**, 242001 (2008) [arXiv:0802.2470 [hep-ph]].
- [95] J. F. Gunion, H. E. Haber and J. Wudka, Phys. Rev. D **43**, 904 (1991).
- [96] M. E. Machacek and M. T. Vaughn, Nucl. Phys. B **222**, 83 (1983); *ibid.* **236**, 221 (1984); *ibid.* **249**, 70 (1985).
- [97] F. Staub, Comput. Phys. Commun. **185**, 1773 (2014) [arXiv:1309.7223 [hep-ph]]; <https://sarah.hepforge.org/>